TECHNISCHE UNIVERSITÄT WIEN
Vienna University of Technology

RESEARCH REPORT

"INFLUENCE OF CARBON MONOXIDE ON THE STRUCTURE AND EXTINCTION BEHAVIOR OF METHANE FLAMES"

Advisors:

Ao. Univ-Prof. Dipl.-Ing. Dr.techn. Ernst Pucher
Institute for Powertrains and Automotive Technology
Vienna University of Technology

and

Prof. Dr. Kalyanasundaram Seshadri
Department of Mechanical and Aerospace Engineering
University of California, San Diego.

Georg Katzlinger

San Diego, July 2013

Abstract

The increasing use of natural gas and biogas as an energy source has fostered the interest in understanding the chemical-kinetical part of the combustion process. Biogas mainly composes of methane, hydrogen and carbon monoxide. As previous research of the combustion group at UC San Diego was already done on hydrogen addition to methane flames, the interest of the research group was now to further the knowledge on the combustion behavior of methane flames under the influence of carbon monoxide.

The research was conducted on a counterflow apparatus in which two opposing, well balanced streams, one being the fuel flux, the other one the oxidizer flux, created a stagnation plane at which the stoichiometric conditions enabled the mixture to keep a stable flame.

Carbon monoxide was separately added to either the fuel or the oxidizer stream. The parameters stoichiometric mixture fraction Z_{st} and adiabatic flame temperature T_{ad} were hereby kept constant. The determining variable was the mass fraction of CO Y_{CO}. The resulting variable was the extinction strain rate of the oxidizer stream $a_{e,O}$.

Unlike the results of the research done on hydrogen addition, which suggested that the influence of hydrogen to methane diffusion flames affects the extinction strain rates in a way irrespective of whether the hydrogen is added on the fuel or oxidizer side (provided that the stoichiometric mixture fraction, the adiabatic flame temperature and the ratio r of the oxidizer flux that burns hydrogen to the oxidizer flux that burns methane are constant), the methane flame under carbon monoxide addition behaves very differently.

Adding carbon monoxide to the oxidizer stream doesn't influence the oxidizer extinction strain rate whereas the CO-addition on the fuel side first increases the oxidizer extinction strain rate and then sharply reduces it after peaking out. This experimental data is qualitatively backed by computational simulations in ChemkinPro.

Table of Contents

I. List of Symbols

A	Pre-exponential Factor for Arrhenius Equation
A'	Temperature-dependent pre-exponential Factor for Arrhenius Equation
CH_4	Methane
C_i	Molar Concentration of i
D	Mass Diffusivity
E_A	Activation Energy
E_b	Activation Energy for backward reactions
E_f	Activation Energy for forward reactions
$H^{\circ}(\mathrm{x})$	Latent Heat at x Kelvin
H_2	Hydrogen
H_i	Molar Enthalpy of species i
L	Distance between duct exits
Le	Lewis-Number
$\overline{\mathrm{M}}_{\mathrm{n}}$	Mean Molecular Weight
N_2	Nitrogen
O_2	Oxygen
Pr	Prandtl-Number
Q_i	Heat Release per consumed mole of species i
Q_p	Heat Transfer
S	Entropy
Sc	Schmidt-Number
SLM	Standard Liters per Minute
T	Temperature
$T_{F,O}$	Temperature at the fuel duct exit
$T_{O,O}$	Temperature at the oxidizer duct exit
T_{ad}	Adiabatic Flame Temperature
T_c	Corrected Gas Temperature
T_f	Flame Temperature
V	Velocity at Duct Exit
W_i	Molecular Weight of i
X	Mole Fraction
Y	Mass Fraction

Z_{st}	Stoichiometric Mixture Fraction
a_E	Extinction Strain Rate
a_I	Ignition Strain Rate
a	Strain Rate
c_p	Specific Heat Capacity at constant pressure
d	Bead Diameter
k_i	Rate Constant of i
$\dot{m}$	Duct Mass Flow
p	Pressure
$\hat{x}$	Axial Coordinate measured from the stagnation plane
α	Thermal Conductivity
ΔH_f°	Heat of Formation at 298K
ΔH	Heat of Reaction
ε	Emissivity
θ	Non-Dimensional Temperature
λ	Thermal Conductivity
ν	Stoichiometric Coefficient
ρ	Density
σ	Boltzmann Constant
ω_i	Reaction Rate of i

II. Subscripts

CO	Carbon-Monoxide-related
F	Fuel-related
u	Unburnt
CH_4	Methane-related
O_2	Oxygen-related
1	Conditions at the fuel duct exit
2	Conditions at oxidizer duct exit

1 Introduction

As a consequence of the ever increasing need for mobility and the subsequent increase in total emissions, emission regulations on vehicles are becoming stricter and stricter. One way car manufacturers try to meet those requirements is to develop alternative/hybrid fuel systems which are partly favored in the aforementioned emission regulations by e.g. longer transition phases or later installment deadlines. One of those alternative fuels is natural gas respectively producer gas/biogas. Natural Gas is currently available at attractive prices due to new drilling techniques and new resource finds in the North American continent. At current low natural gas prices, costs per mile are less than half of those using gasoline vehicles. This makes natural gas an attractive fuel for cars in the U.S., and many buses, fleets, and personal cars have been either converted to accept CNG (compressed natural gas), or been replaced with CNG vehicles. Natural gas has a reputation as clean-burning fuel.

The main impact is that many gasoline-vehicles can be replaced with natural gas-fuelled vehicles. In a next step, natural gas can be replaced by producer gas/biogas. Producer gas is an artificially manufactured gas composed of mainly methane, carbon monoxide, hydrogen and carbon dioxide. It can be produced through gasification of organic materials. Very often producer gas as well as gas obtained from fermentation is described by the umbrella term biogas.

The main purpose of this research work was to further develop the understanding of how the flame structure and extinction behavior of a methane flame changes over varying the point of addition of carbon monoxide as well as varying the mixtures composition. Similar research was already done in a recent study conducted by the Combustion Research Group at the University of California San Diego. The effects on extinction when adding hydrogen (H_2) to a stream of methane (CH_4) were examined. The research was conducted on a counterflow apparatus in which two opposing, well balanced streams, one being the fuel flux, the other one the oxidizer flux, created a stagnation plane at which the stoichiometric conditions enabled the mixture to keep a stable flame.

In the course of the experiment hydrogen was added sequentially to either of the two streams varying the mass fraction of the hydrogen Y_{H_2}. The criterion was to measure at which set level of mass fractions the flame would extinct by varying the strain rate of the fluxes. These measurements were conducted for both adding the hydrogen on the oxidizer side and on the fuel side.

The result of this study suggested that the influence of hydrogen addition to methane diffusion flames affects the extinction strain rates in a way irrespective of whether the hydrogen is added on the fuel or oxidizer side, provided that the stoichiometric mixture fraction, the adiabatic flame temperature and the ratio r of the oxidizer flux that burns hydrogen to the oxidizer flux that burns

methane are constant. In other words, the three parameters stoichiometric mixture fraction Z_{st}, adiabatic stoichiometric temperature T_{ad} and R determine the extinction strain rate uniquely, whether the hydrogen is added to the fuel or oxidizer stream. [1]
In methane flames the methane usually gets consumed in a very narrow area, called the fuel-consumption zone where at the same time hydrogen and carbon monoxide originate. Both intermediate species hydrogen and carbon monoxide get subsequently consumed in the oxygen-consumption zone. Because of the two-layer structure of the reaction zone it is unclear in advance whether addition of the intermediate to one stream will have the same effect as its addition to the other. [1]

In that sense both hydrogen and carbon monoxide prove to be of special interest which leads to the purpose of this diploma thesis: The detailed analysis of the influence of carbon monoxide on the extinction behavior of an Equidiffusional Diffusion Flame. [1]

The practical relevance of this study can easily be found when having a closer look on producer gas combustion. Even though the composition of producer gases can vary in a wide range, measurements at the pilot-gasification plant at the Woodland Biomass Research Center (WBRC) have shown that the mole fraction of CO can make up for 30,5% of the gas composition whereas that of CH_4 accounts for 17%. The potentially strong influence on the combustion process is obvious. The present work aims to improve the basic knowledge of the associated trade-offs between fuel-side and oxidizer-side addition of the reactant carbon monoxide participating in the original diffusion flame.

To better understand the theoretical principles underlying this research a short introduction into producer gases and syngases, the extinction and autoignition behavior of flames described by the so called “S-Shaped Curve”, and the Arrhenius equation describing the reactive behavior are given in this chapter.

1.1 Producer Gas/Syngas

Producer Gas respectively Syngas is basically the result of directed incomplete combustion of carbonaceous fuels. The process of gasification involves converting organic fuels (i.e. biomass) into the producer gas/syngas in an oxygen-lean environment. This lack of oxygen described by the equivalence ration leads to the incomplete combustion. The following reaction describes the process:

$$\boldsymbol{Biomass + Limited\ Air \rightarrow Carbon\ Monoxide + Hydrogen + Methane + Carbon\ Dioxide + Water\ Vapor + Nitrogen}$$

The difference between Producer Gas and Syngas is the composition respectively the path of production. Producer Gas is composed of carbon monoxide, hydrogen, carbon dioxide, nitrogen and several hydrocarbons such as methane. Syngas on the other side is mainly a mixture of carbon monoxide and hydrogen as a result of high-temperature gasification of organic material. Through the Fischer-Tropsch synthesis as well as previously necessary clean-ups of the syngas to remove impurities, synthetic Diesel can be produced. [2]

The gasification of producer gases occurs at temperatures in between 1110°F and 2730°F depending on the process type and general conditions (e.g. pressure, equivalence ratio, fluidization speed) and yields low to medium-energy content gases. While gasification, the biomass resource (i.e. the fuel) is heated up to high temperatures where decomposition in volatile compounds (gases) and solid residues (char) takes place. The exact composition hereby depends on the reactor temperature and type. The major and most commonly used type hereby is the Fixed Bed Gasification Reactor. [3], [4]

Fixed bed reactors are usually very durable due to their low level of erosion of the reactor materials and comparably simple to operate. The fuels in fixed bed reactors move either antiparallel or parallel to the stream of the gasification medium (Air, steam, or O_2) as the fuel is converted to fuel gas. There are three basic fixed bed designs – updraft, downdraft and cross-draft gasifiers. [5]

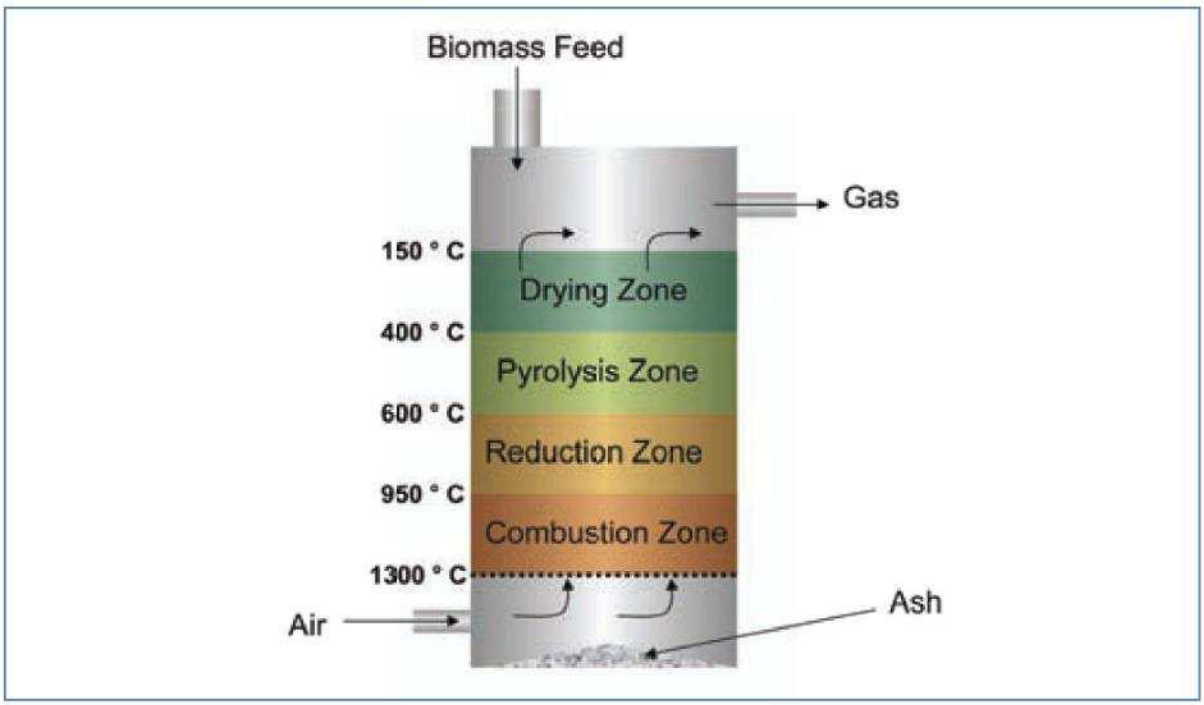

Figure 1.1: An updraft Fixed Bed Gasifier has an antiparallel flow of the gas and the fuel to each other. The gasification medium (Air, Steam or O_2) is added at the bottom of the reactor and ascends to the top. The fuel is descends from the top to the bottom through zones of progressively increasing temperatures. [5]

Updraft gasification is a widely used system to gasify biomass resources by the use of steam as the reactive agent. Certain attention has to be paid to slagging if high ash fuels are used.

By rising heat from the combustion zone upward, energy is provided for the pyrolysis and drying zones. Gases, tar and other aerosols are skimmed at the top of the reactor while ash is removed at the bottom. The produced gas typically contains high levels of tar, which must be removed or further converted to syngas for use in applications other than direct heating. [3], [4]

2 Experimental Parameters

Measuring the influence of CO addition to different fluxes and comparing the results required certain parameters to be fixed. Since reaction rates prove to have a strong temperature dependency it was advantageous to keep the adiabatic flame temperature T_{ad} fixed. Not doing this would have caused different reaction-zone temperatures to dominate the results.
The second parameter to keep fixed was the stoichiometric mixture fraction Z_{st}. Making comparisons at fixed values of Z_{st} is desirable as the variations in structure of reaction zones can be eliminated. [1]

The variable parameters were the CO mass fraction Y_{CO} respectively the strain rate of the oxidizer stream a_O. By choosing the CO mass fraction Y_{CO} the remaining components' mass fractions could be defined. The asymptotical approach for defining the the components' mass fractions is based on the mathematical model developed for the corresponding research on hydrogen addition. It was adopted to the addition of carbon monoxide.
The variable parameter strain rate a_O finally defined the exact fluxes of the mixture components at the oxidizer duct exit. Through the constraint of the momentum balance at the stagnation plane it also defined the strain rate and the fluxes at the fuel duct exit.

The approach used throughout this work is that of non-premixed combustion in a laminar counterflow apparatus. The counterflow burner in use is a well established instrument and based on the principles of the one described in [6]. In practical applications like diesel engines, the fuel and the oxidizer are mixed to a burnable regimen through diffusion. By applying Prandtl's boundary layer approximation on the counterflow setup this originally three-dimensional problem can be reduced to a one-dimensional. The assumption of Prandtl's theory is that the diffusion into the direction orthogonal to the stream line can be neglected. This leaves the axis orthogonal to the stagnation plane as the single spatial variable.

By further using the assumptions that

- the temperature and mass fractions are functions only dependent on the x-axis normal to the stagnation plane
- the velocity v_x is a function of the x-axis only
- the tangential velocity v_y is proportional to the coordinate y tangential to the flame level, $v_y = Ky$

the system can be further reduced and simplified to be of steady state ($\frac{\partial}{\partial t} = 0$). [7]

2.1 Fixed Parameters

2.1.1 Stoichiometric Mixture Fraction Z_{st}

The Mixture Fraction Z is a very useful variable when it comes to diffusion flame combustion. The equations presented in this paragraph describe the conditions in a homogeneous system. By postulating perfect combustion in this diffusional counterflow setup, a homogeneous mixture can be assumed in the reaction zone and hence this mathematical definition applied. The fuel flux (index 1) with the mass flow $\dot{m}_1$ is mixed with an oxidizer flux (index 2) with the mass flow $\dot{m}_2$. The mixture fraction represents the mass fraction of the fuel flux of the gas mixture. This can be calculated by

$$Z = \frac{\dot{m}_1}{\dot{m}_1 + \dot{m}_2} \tag{2.1}$$

Both the fuel and the oxidizer flux can hereby contain inert gases like for example nitrogen. The mass fraction of the fuel in the mixture is proportional to the mass fraction of the fuel in the fuel stream given by

$$Y_{F,u} = Y_{F,1} Z \tag{2.2}$$

The mass fraction of the oxidizer in the mixture can be similarly calculated by applying its mass fraction $(1 - Z)$ in the equation

$$Y_{O_2,u} = Y_{O_2,2}(1 - Z) \tag{2.3}$$

$Y_{O_2,2}$ is the mass fraction of the oxygen in the oxidizer stream ($Y_{O_2,2} = 0.232$ resp $X_{O_2,2} = 0.21$ in air). Combining equations (2.2) and (2.3) and inserting them in the equation for a stoichiometric fuel-oxidizer mixture

$$\nu Y_F - Y_{O_2} = \nu Y_{F,u} - Y_{O_2,u} \tag{2.4}$$

with $\nu Y_F = Y_{O_2}$ the following definition for the stoichiometric mixture fraction can be obtained

$$Z_{st} = \left[1 + \frac{\nu Y_{F,1}}{Y_{O_2,2}}\right]^{-1} \tag{2.5}$$

The mixture fraction Z_{st} was chosen to be 0.055 according to previous studies [8] and [9].

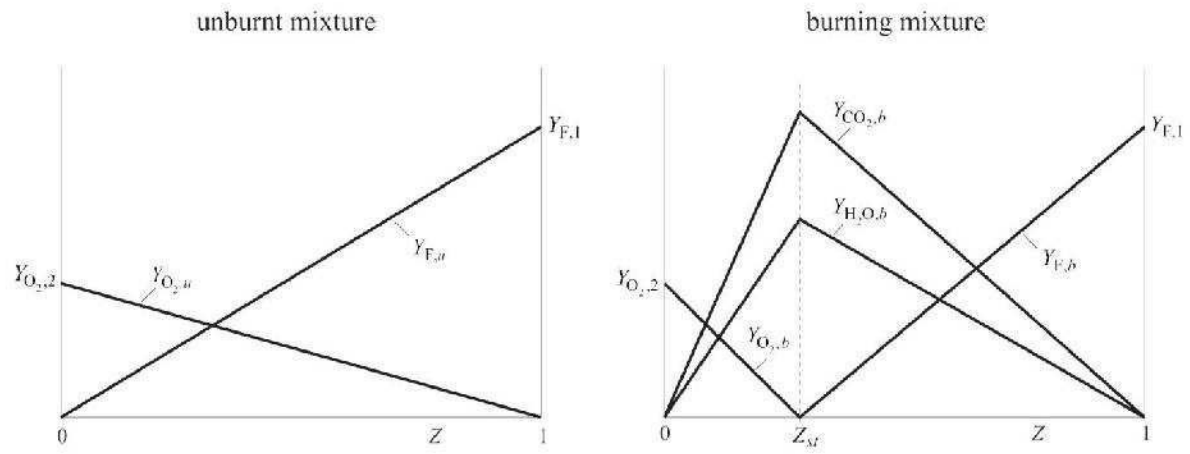

Figure 2.1: Profiles of Y_F, Y_{O2} and Y_{H2O} in the unburnt and burning gas mixture.

Figure 2.1 graphically shows the idea, that at the stoichiometric mixture fraction Z_{st} all of the oxygen $Y_{O_2,2}$ and all of the added fuel $Y_{F,1}$ gets consumed and reacts to its products carbon monoxide Y_{CO_2},b and hydrogen $Y_{H_2O,b}$.

2.1.2 Adiabatic Flame Temperature T_{ad}

The adiabatic flame temperature T_{ad} describes the theoretical flame temperature of the mixture that can be reached when being combusted. In this research work two adiabatic flame temperatures were being investigated: 2000K and 2100K. Assuming a constant adiabatic flame temperature means that all the heat evolved is used to raise the temperature of the product gases. This equals to a constant enthalpy of the system ($\Delta H = 0$) and no heat transfer in and out of the system ($Q_p = 0$).
Since the adiabatic flame temperature of the mixture as well as the enthalpy of the system is directly determined by the mixture components, its mass fractions and its specific heat capacities, the mass fractions for the two cases of $T_{ad} = 2000K$ and $T_{ad} = 2100K$ differ considerably as can be seen in *Table 2.1 - Table 2.4*.

2.2 Variable Parameters

2.2.1 Strain Rate

The strain rate is defined as the normal gradient of the normal component of the flow velocity and is calculated by the equation

$$a_2 = \frac{2|V_2|}{L}\left(1 + \frac{|V_1|\sqrt{\rho_1}}{|V_2|\sqrt{\rho_2}}\right) \tag{2.6}$$

V_1 and V_2 are both the normal components of the flow velocities from the fuel stream (index 1) and the oxidizer stream (index 2). The variables ρ_1 and ρ_2 refer to the densities of the two streams accordingly. L represents the distance between the exits of the two ducts. The equation is obtained from an asymptotic approach where the Reynolds numbers of the fluxes at the duct exists are presumed to be large. [10]

Further applying the constraint of momentum balance (as described in 3.2.4 Counterflow Burner) on the previous equation, the following simplification can be obtained.

$$a_2 = \frac{4|V_2|}{L} \tag{2.7}$$

The strain rate in general is an appropriate parameter to describe the flame behavior especially in the field of diffusion flame combustion. In a pure diffusion flame the strain rate can be defined by calculating the velocity gradients in the flow field. In regions of high strain rates fluid shear, mixing rates and bulk transport rates are faster than chemical reaction rates, thus local reactions are not allowed to go to completion before the flow carries the combustion radicals away from the reaction zone. The net result of this process is a reduction in peak flame temperature of a highly strained flame, which in return e.g. reduces thermal NO_x production. This points to increased strain rates as a possible path to reducing or effectively eliminating thermal NO_x in a diluted diffusion flame for example.

2.2.2 Asymptotical Model for Calculating the Mass Fractions

2.2.2.1 Chemical Reaction

The chemical reaction between CH_4 and O_2 is described by the simple one-step process

$$\boldsymbol{CH_4 + 2O_2 \rightarrow CO_2 + 2H_2O}$$

The reaction rate ω_F is

$$\omega_F = C_F C_{O2} k_F \tag{2.8}$$

where k_F is the rate constant, C_F is the molar concentration of fuel and C_{O_2} the molar concentration of oxygen. The chemical reaction between CO and O2 is

$$\mathrm{CO} + (\frac{1}{2})\mathrm{O_2} \rightarrow \mathrm{CO_2}$$

The reaction rate ω_{CO} is

$$\omega_{CO} = C_{CO} C_{O2} k_{CO} \tag{2.9}$$

where k_{CO} is the rate constant, C_{CO} is the molar concentration of carbon monoxide. It follows that

$$\begin{aligned} C_F &= \rho \frac{Y_F}{W_F} \\ C_{CO} &= \rho \frac{Y_{CO}}{W_{CO}} \\ C_{O2} &= \rho \frac{Y_{O2}}{W_{O2}} \end{aligned} \tag{2.10}$$

Here ρ is the density of the mixture, Y_F, Y_{CO} and Y_{O2} are the mass fractions of CH4, CO and O2 respectively, and W_F, W_{CO} and W_{O2} are the molecular weights.

2.2.2.2 Formulation

Consider two counterflowing streams flowing toward a stagnation plane. One stream called fuel stream is made up of CH4 and N2 and the other stream, called the oxidizer stream, is made up of O_2 and N_2. Carbon Monoxide is added to the fuel stream or to the oxidizer stream. The mass fraction of CH_4 in the fuel stream is $Y_{F,1}$ and that of O_2 in the oxidizer stream is $Y_{O_2,2}$. When CO is added to the fuel stream its mass fraction in the fuel stream is $Y_{CO,1}$ and it is $Y_{CO,2}$ when added to the oxidizer stream. For inviscid flow, with equal velocity and density of the counterflowing streams, the axial component of the flow velocity is $v = -a * \hat{x}$, where a is the strain rate, and $\hat{x}$ the axial coordinate measured from the stagnation plane. The species balance equations are

$$\begin{aligned} \rho a\hat{x}\frac{dY_F}{d\hat{x}} + \rho D_F\frac{d^2Y_F}{d\hat{x}^2} &= W_F\omega_F \\ \rho a\hat{x}\frac{dY_{CO}}{d\hat{x}} + \rho D_{CO}\frac{d^2Y_{CO}}{d\hat{x}^2} &= W_{CO}\omega_{CO} \\ \rho a\hat{x}\frac{dY_{O2}}{d\hat{x}} + \rho D_{O2}\frac{d^2Y_{O2}}{d\hat{x}^2} &= 2W_{O2}\omega_F + (\frac{1}{2})W_{O2}\omega_{CO} \end{aligned} \tag{2.11}$$

Here D_F, D_{CO} and D_{O2} are the coefficients of diffusion of CH_4, CO and O_2 respectively. The energy conservation equation is

$$\rho c_p a\hat{x}\frac{dT}{d\hat{x}} + \lambda\frac{d^2T}{d\hat{x}^2} + \sum_{i=1}^{n}(\rho D_i c_{p,i}\frac{dY_i}{d\hat{x}}\frac{dT}{d\hat{x}}) = -Q_F\omega_F - Q_{CO}\omega_{CO} \tag{2.12}$$

Here λ is the coefficient of thermal conductivity, c_p is the heat capacity of the mixture, $c_{p,i}$ is the heat capacity of species i, D_i is the coefficient of diffusion of species i, Q_F is the heat released per mole of CH_4 consumed and Q_{CO} is the heat released per mole of CO consumed. Defining the independent variable

$$x = \hat{x}(\rho C_p\frac{a}{\lambda})^{\frac{1}{2}} \tag{2.13}$$

where C_p is the heat capacity and λ the thermal conductivity, the normalized mass fractions are

$$\begin{aligned} y_F &= \frac{2Y_F W_{O2}}{Y_{O2,2}W_F} \\ y_{CO} &= \frac{Y_{CO}W_{O2}}{2Y_{O2,2}W_{CO}} \\ y_{O2} &= \frac{Y_{O2}}{Y_{O2,2}} \end{aligned} \tag{2.14}$$

The non-dimensional temperature, θ, is

$$\theta = \frac{2c_p W_{O2}(T - T_u)}{Q_F Y_{O2,2}} \tag{2.15}$$

Here T_u is the temperature of the reactant streams at $\pm\infty$.

Introducing equations (2.8), (2.9), (2.10), (2.13) and (2.14) into Equation (3.4) gives

$$\begin{aligned} x\frac{dy_F}{dx} + \frac{1}{Le_F}\frac{d^2y_F}{dx^2} &= \Delta_F y_F y_{O2} \\ x\frac{dy_{CO}}{dx} + \frac{1}{Le_{CO}}\frac{d^2y_{CO}}{dx^2} &= \Delta_{CO} y_{CO} y_{O2} \\ x\frac{dy_{O2}}{dx} + \frac{1}{Le_{O2}}\frac{d^2y_{O2}}{dx^2} &= \Delta_F y_F y_{O2} + \Delta_{CO} y_{CO} y_{O2} \end{aligned} \tag{2.16}$$

where

$$\begin{aligned} Le_F &= \frac{\lambda}{\rho C_p D_F} \\ Le_{O2} &= \frac{\lambda}{\rho C_p D_{O2}} \\ Le_{CO} &= \frac{\lambda}{\rho C_p D_{CO}} \end{aligned} \tag{2.17}$$

are the respectively Lewis numbers of CH_4, CO and O_2. The values of these quantities are presumed to be constant. The Damköhler numbers Δ_F and Δ_{CO} are defined as

$$\begin{aligned} \Delta_F &= \frac{\rho k_F Y_{O2,2}}{\alpha W_{O2}} \\ \Delta_{CO} &= \frac{\rho k_{CO} Y_{O2,2}}{\alpha W_{O2}} \end{aligned} \tag{2.18}$$

For simplicity the approximation

$$Le_F = Le_{O2} = Le_{CO} = 1 \tag{2.19}$$

is introduced because the values of these quantities are very close to unity.

Introducing equations (2.8), (2.9), (2.10), (2.13), (2.14) and (2.15) into equation (2.12) and using Equation (2.18), the following equation is obtained for θ

$$x\frac{d\theta}{dx}+\frac{d^2\theta}{dx^2}=-\Delta_F y_F y_{O2}-\alpha\Delta_{CO}y_{CO}y_{O2} \tag{2.20}$$

The quantity α is defined as

$$\alpha=\frac{4Q_{CO}}{Q_F} \tag{2.21}$$

Equation (2.20) is constrained to satisfy the condition

$$\theta=0 \quad \text{at} \quad x=\pm\infty \tag{2.22}$$

The conserved scalar quantities Z is defined by the equation

$$x\frac{dZ}{dx}+\frac{d^2Z}{dx^2}=0 \tag{2.23}$$

Equation (2.23) is constrained to satisfy the conditions

$$Z=0 \quad \text{at} \quad x=\infty \tag{2.24}$$

Integration of equation (2.23) together with equation (2.24) gives

$$Z=\frac{1}{2}erfc\left(x\sqrt{\frac{1}{2}}\right) \tag{2.25}$$

Introducing equation (2.23) into equations (2.16) and (2.20) gives

$$\begin{aligned}
\frac{d^2y_F}{dZ^2}&=\Delta_F\left(\frac{dZ}{dx}\right)^{-2}y_F y_{O2}\\
\frac{d^2y_{CO}}{dZ^2}&=\Delta_{CO}\left(\frac{dZ}{dx}\right)^{-2}y_{CO}y_{O2}\\
\frac{d^2y_{O2}}{dZ^2}&=\Delta_F\left(\frac{dZ}{dx}\right)^{-2}y_F y_{O2}+\Delta_{CO}\left(\frac{dZ}{dx}\right)^{-2}y_{CO}y_{O2}\\
\frac{d^2\theta}{dZ^2}&=-\Delta_F\left(\frac{dZ}{dx}\right)^{-2}y_F y_{O2}-\alpha\Delta_{CO}\left(\frac{dZ}{dx}\right)^{-2}y_{CO}y_{O2}
\end{aligned} \tag{2.26}$$

2.2.2.3 Outer Structure

Let the flame be located at $Z = Z_{st}$. At the reaction zone,

$$\begin{aligned} y_F = y_{CO} = y_{O2} = 0 \\ \theta = \theta_{st} = \frac{2c_p W_{O2}(T_{st} - T_u)}{Q_F Y_{O2,2}} \end{aligned} \tag{2.27}$$

Here the quantity T_{st} is the adiabatic temperature. The gradients at Z_{st+} are

$$\begin{aligned} \frac{dy_F}{dZ} &= \frac{2Y_{F,1}W_{O2}}{Y_{O2,2}W_F}\frac{1}{(1-Z_{st})} \\ \frac{dy_{CO}}{dZ} &= \frac{Y_{CO,1}W_{O2}}{2Y_{O2,2}W_{CO}}\frac{1}{(1-Z_{st})} \\ \frac{d\theta}{dZ} &= -\frac{2c_p W_{O2}(T_{st}-T_u)}{Y_{O2,2}Q_F}\frac{1}{(1-Z_{st})} \end{aligned} \tag{2.28}$$

The gradients at Z_{st-} are

$$\begin{aligned} \frac{dy_{O2}}{dZ} &= -\frac{1}{Z_{st}} \\ \frac{dy_{CO}}{dZ} &= -\frac{Y_{CO,2}W_{O2}}{2Y_{O2,2}W_{CO}}\frac{1}{Z_{st}} \\ \frac{d\theta}{dZ} &= \frac{2c_p W_{O2}(T_{st}-T_u)}{Y_{O2,2}Q_F}\frac{1}{Z_{st}} \end{aligned} \tag{2.29}$$

The following coupling relations are obtained

$$\begin{aligned} \frac{d^2}{dZ^2}(y_F + y_{CO} - y_{O2)} = 0 \\ \frac{d^2}{dZ^2}[(1-\alpha)y_F + \alpha y_{O2} + \theta] = 0 \end{aligned} \tag{2.30}$$

These coupling relations are applied in the reaction zone at $Z = Z_{st}$. Integrating these coupling relations once and matching with the slopes in the region $Z < Z_{st}$ and $Z > Z_{st}$ given by equations (2.28) and (2.29) the following two relations are obtained.

$$\frac{2Y_{F,1}}{W_F} + \frac{Y_{CO,1}}{2W_{CO}} = \left[\frac{Y_{O2,2}}{W_{O2}} - \frac{Y_{CO,2}}{2W_{CO}}\right]\frac{(1-Z_{st})}{Z_{st}} \tag{2.31}$$

$$-\frac{2c_p(T_{st}-T_u)}{Q_F}+\frac{2Y_{F,1}}{W_F}+\alpha\frac{Y_{CO,1}}{2W_{CO}}=\left[\frac{2c_p(T_{st}-T_u)}{Q_F}-\alpha\frac{Y_{CO,2}}{2W_{CO}}\right]\frac{(1-Z_{st})}{Z_{st}} \tag{2.32}$$

Equation (2.32) can be further simplified to give

$$c_p(T_{st}-T_u)=\frac{Y_{F,1}Q_FZ_{st}}{W_F}+\frac{Q_{CO}}{W_{CO}}\left[Y_{CO,1}Z_{st}+Y_{CO,2}(1-Z_{st})\right] \tag{2.33}$$

Enthalpies of formation at 298K for CH_4, CO, CO_2 and H_2O are -74,873kJ/mol, -110,527kJ/mol, -393,522kJ/mol, -241,826kJ/mol respectively as stated in *3.1 Chemical Components*.

The Released Heat Q_F is calculated by $Q_F=(393{,}52+2*241{,}83-74{,}9)*1000=802280J/mol$. Hence $Q_{CO}=(393{,}52-110{,}53)*1000=282990J/mol$. It follows that $\alpha=4\frac{Q_{CO}}{Q_F}=1{,}41$.

2.2.2.4 Coupling Relations

For convenience the quantity X_i is defined as

$$X_i=\frac{Y_iW_{N2}}{W_i} \tag{2.34}$$

Conservation of the element carbon, hydrogen and oxygen give

$$\begin{gathered}X_F+X_{CO2}+X_{CO}=X_{CO,2}(1-Z)+\left(X_{F,1}+X_{CO,1}\right)Z\\2X_F+X_{H2O}=2X_{F,1}Z\\2X_{O2}+X_{CO}+2X_{CO2}+X_{H2O}=(2X_{O2,2}+X_{CO,2})(1-Z)+X_{CO,1}Z\end{gathered} \tag{2.35}$$

and energy conservation gives

$$\sum_i X_iH_i-\left[X_{F,1}H_FT_u+X_{CO,1}H_{CO}T_u\right]Z-\left[X_{O2,2}H_{O2}T_u+X_{CO,2}H_{CO}T_u\right](1-Z)=0 \tag{2.36}$$

Here H_i is the molar enthalpy of species i and $T_u=T_2+(T_1-T_2)$. At $Z=Z_{st}$, $X_F=X_{O2}=X_{CO}=0$. As a consequence the following relations are obtained from the first two relations in Equation (2.35)

$$\begin{gathered}X_{CO2,st}=X_{CO,2}+\left(X_{CO,1}-X_{CO,2}\right)Z_{st}+X_{F,1}Z_{st}\\X_{H2O,st}=2X_{F,1}Z_{st}\end{gathered} \tag{2.37}$$

It follows from Equation (2.37) that

$$X_{N2,st} = Y_{N2,st} = 1 - \frac{X_{CO2,st} W_{CO2}}{W_{N2}} - \frac{X_{H2O,st} W_{H2O}}{W_{N2}} \tag{2.38}$$

Here $X_{CO2,st}$ and $X_{H2O,st}$ are the values of X_{CO2} and X_{H2O} at $Z = Z_{st}$. The value of Z_{st} is obtained from the last relation in Equation (2.35)

$$X_{CO,2} + \left(X_{CO,1} - X_{CO,2}\right) Z_{st} + 4X_{F,1} Z_{st} = 2X_{O2,2}(1 - Z_{st}) \tag{2.39}$$

where use is made of Equation (2.37) and Equation (2.39) is rewritten as

$$Z_{st} = \frac{2X_{O2,2} - X_{CO,2}}{2X_{O2,2} - X_{CO,2} + X_{CO,1} + 4X_{F,1}} \tag{2.40}$$

The caloric equation $H_i(T) = H_i(T_O) + W_i \int_{T_o}^{T} c_{p,i} dT$, where $c_{p,i}$ is the heat capacity per unit mass of species i and T_0 is the reference temperature. In the present formulation $T_0 = T_u = T_1 = T_2$. It follows from Equation (2.36) that

$$\begin{aligned} &\int_{T_u}^{T_{st}} \left(Y_{CO2,st} c_{p,CO2} + Y_{H2O,st} c_{p,H2O} + Y_{N2,st} c_{p,N2}\right) dT \\ &\qquad = \frac{Q_F Y_{F,1} Z_{st}}{W_F} + \frac{Q_{CO} Y_{CO,1} Z_{st}}{W_{CO}} + \frac{Q_{CO} Y_{CO,2}(1 - Z_{st})}{W_{CO}} \end{aligned} \tag{2.41}$$

2.2.2.5 Summary

In the course of this experiment the variables $Z_{st} = 0{,}055$, $T_{st,1} = 2100K$, $T_{st,2} = 2100K$ and $T_u = 298K$ were pre-selected. With $Z_{st} = 0{,}055$ a relation between $Y_{F,ref}$ and $Y_{O2,ref}$ is given by

$$Z_{st} = \left(1 + \frac{4Y_{F,ref}}{Y_{O2,ref}}\right)^{-1} \tag{2.42}$$

The stoichiometric relation for the basic reaction is

$$\boldsymbol{CH_4 + 2O_2 + a_{N2}N_2 \rightarrow CO_2 + 2H_2O + a_{N2}N_2}$$

Here

$$a_{N2} = a_{F,N2} + a_{ox,N2} \tag{2.43}$$

By defining the variables

$$\begin{aligned} Y_{F,ref} &= \frac{16}{16 + 28a_{F,N2}} \\ Y_{O2,ref} &= \frac{64}{64 + 28a_{F,N2}} \end{aligned} \tag{2.44}$$

and choosing the number of moles $a_{F,N2}$ and $a_{ox,N2}$ in a way that the criteria $T_{st,1} = 2100K$, $T_{st,2} = 2100K$ and $Z_{st} = 0{,}055$ are met, an initial guess for $c_p(T, Y_i)$ can be calculated by using the relation

$$c_p = \frac{Y_{F,ref} Z_{st} Q_F}{W_F (T_{st} - T_u)} \tag{2.45}$$

where $Q_F = 802570J/mol$ is the heat release per mole of CH_4 consumed. Molecular weights are $W_F = 0{,}016kg/mol$, $W_{O_2} = 0{,}032kg/mol$ and $W_{CO} = 0{,}028kg/mol$. The unit of c_p in this calculation is J/(kg*K).

2.2.3 Calculated Mass Fractions

2.2.3.1 CO addition on air side

A value is being selected for $Y_{CO,2}$. The value of $Y_{F,1}$ is obtained from

$$Y_{F,1} = \frac{W_F}{Q_F Z_{st}} \left[c_p (T_{st} - T_u) - \frac{Q_{CO} Y_{CO,2} (1 - Z_{st})}{W_{CO}} \right] \tag{2.46}$$

The value of $Y_{O2,2}$ is obtained from

$$Y_{O2,2} = W_{O2} \left[\frac{2Y_{F,1}}{W_F} \frac{Z_{st}}{(1 - Z_{st})} + \frac{Y_{CO,2}}{2W_{CO}} \right] \tag{2.47}$$

This leads to the following mass fractions:

Y(CO,2)	Y(O2,2)	Y(N2,2)	Y(Air,2)	Y(F,1)	Y(N2,1)
0,000	0,187	0,813	0,804	0,806	0,194
0,010	0,184	0,806	0,790	0,768	0,232
0,020	0,181	0,799	0,777	0,731	0,269
0,030	0,178	0,792	0,764	0,693	0,307
0,040	0,175	0,785	0,751	0,655	0,345
0,050	0,172	0,778	0,737	0,617	0,383
0,060	0,169	0,771	0,724	0,579	0,421
0,070	0,166	0,764	0,711	0,541	0,459
0,080	0,162	0,758	0,697	0,503	0,497
0,090	0,159	0,751	0,684	0,465	0,535
0,100	0,156	0,744	0,671	0,427	0,573
0,110	0,153	0,737	0,657	0,389	0,611
0,120	0,150	0,730	0,644	0,351	0,649
0,130	0,147	0,723	0,631	0,313	0,687
0,140	0,144	0,716	0,618	0,275	0,725
0,150	0,141	0,709	0,604	0,237	0,763
0,160	0,138	0,702	0,591	0,199	0,801
0,170	0,135	0,695	0,578	0,161	0,839
0,180	0,131	0,689	0,564	0,123	0,877
0,190	0,128	0,682	0,551	0,086	0,914
0,200	0,125	0,675	0,538	0,048	0,952

0,210	0,122	0,668	0,524	0,010	0,990

Table 2.1: Mass Fractions at Duct Exit; CO addition on Oxidizer Side; Adiabatic Flame Temperature: 2000K

Y(CO,2)	Y(O2,2)	Y(N2,2)	Y(Air,2)	Y(F,1)	Y(N2,1)
0,000	0,201	0,799	0,863	0,866	0,134
0,010	0,198	0,792	0,849	0,827	0,173
0,020	0,195	0,785	0,836	0,789	0,211
0,030	0,192	0,778	0,822	0,751	0,249
0,040	0,188	0,772	0,808	0,713	0,287
0,050	0,185	0,765	0,795	0,674	0,326
0,060	0,182	0,758	0,781	0,636	0,364
0,070	0,179	0,751	0,768	0,598	0,402
0,080	0,176	0,744	0,754	0,560	0,440
0,090	0,173	0,737	0,740	0,522	0,478
0,100	0,169	0,731	0,727	0,483	0,517
0,110	0,166	0,724	0,713	0,445	0,555
0,120	0,163	0,717	0,700	0,407	0,593
0,130	0,160	0,710	0,686	0,369	0,631
0,140	0,157	0,703	0,673	0,330	0,670
0,150	0,154	0,696	0,659	0,292	0,708
0,160	0,150	0,690	0,645	0,254	0,746
0,170	0,147	0,683	0,632	0,216	0,784
0,180	0,144	0,676	0,618	0,178	0,822
0,190	0,141	0,669	0,605	0,139	0,861
0,200	0,138	0,662	0,591	0,101	0,899
0,210	0,135	0,655	0,578	0,063	0,937
0,220	0,131	0,649	0,564	0,025	0,975

Table 2.2: Mass Fractions at Duct Exit; CO addition on Oxidizer Side; Adiabatic Flame Temperature: 2100K

2.2.3.2 CO addition on fuel side

A value is being selected for $Y_{CO,1}$. The value of $Y_{F,1}$ is obtained from

$$Y_{F,1} = \frac{W_F}{Q_F Z_{st}}\left[c_p(T_{st} - T_u) - \frac{Q_{CO} Y_{CO,1} Z_{st}}{W_{CO}}\right] \tag{2.48}$$

The value of $Y_{O2,2}$ is obtained from

$$Y_{O2,2} = W_{O2}\left[\frac{2Y_{F,1}}{W_F} + \frac{Y_{CO,1}}{2W_{CO}}\right]\frac{Z_{st}}{(1 - Z_{st})} \tag{2.49}$$

This leads to the following mass fractions:

Y(CO,1)	Y(F,1)	Y(N2,1)	Y(O2,2)	Y(N2,2)	Y(Air,2)
0,000	0,806	0,194	0,187	0,813	0,804
0,010	0,804	0,186	0,187	0,813	0,803
0,020	0,802	0,178	0,187	0,813	0,802
0,030	0,800	0,170	0,187	0,813	0,801
0,040	0,798	0,162	0,187	0,813	0,801
0,050	0,795	0,155	0,186	0,814	0,800
0,060	0,793	0,147	0,186	0,814	0,799
0,070	0,791	0,139	0,186	0,814	0,798
0,080	0,789	0,131	0,186	0,814	0,798
0,090	0,787	0,123	0,186	0,814	0,797
0,100	0,784	0,116	0,185	0,815	0,796
0,110	0,782	0,108	0,185	0,815	0,795
0,120	0,780	0,100	0,185	0,815	0,794
0,130	0,778	0,092	0,185	0,815	0,794
0,140	0,775	0,085	0,185	0,815	0,793
0,150	0,773	0,077	0,185	0,815	0,792
0,160	0,771	0,069	0,184	0,816	0,791
0,170	0,769	0,061	0,184	0,816	0,791
0,180	0,767	0,053	0,184	0,816	0,790
0,190	0,764	0,046	0,184	0,816	0,789
0,200	0,762	0,038	0,184	0,816	0,788
0,210	0,760	0,030	0,183	0,817	0,787

0,220	0,758	0,022	0,183	0,817	0,787
0,230	0,756	0,014	0,183	0,817	0,786
0,240	0,753	0,007	0,183	0,817	0,785

Table 2.3: Mass Fractions at Duct Exit; CO addition on Fuel Side; Adiabatic Flame Temperature: 2000K

Y(CO,1)	Y(F,1)	Y(N2,1)	Y(O2,2)	Y(N2,2)	Y(Air,2)
0,000	0,866	0,134	0,201	0,799	0,863
0,010	0,863	0,127	0,201	0,799	0,862
0,020	0,861	0,119	0,201	0,799	0,861
0,030	0,859	0,111	0,200	0,800	0,860
0,040	0,857	0,103	0,200	0,800	0,859
0,050	0,854	0,096	0,200	0,800	0,859
0,060	0,852	0,088	0,200	0,800	0,858
0,070	0,850	0,080	0,200	0,800	0,857
0,080	0,848	0,072	0,200	0,800	0,856
0,090	0,846	0,064	0,199	0,801	0,856
0,100	0,843	0,057	0,199	0,801	0,855
0,110	0,841	0,049	0,199	0,801	0,854
0,120	0,839	0,041	0,199	0,801	0,853
0,130	0,837	0,033	0,199	0,801	0,852
0,140	0,834	0,026	0,198	0,802	0,852
0,150	0,832	0,018	0,198	0,802	0,851
0,160	0,830	0,010	0,198	0,802	0,850
0,170	0,828	0,002	0,198	0,802	0,849

Table 2.4: Mass Fractions at Duct Exit; CO addition on Fuel Side; Adiabatic Flame Temperature: 2100K

2.2.3.3 Calculation of c_p

The quantities $Y_{CO2,st}$ and $Y_{H2O,st}$ are

$$Y_{CO2,st} = W_{CO2}\left[\frac{Y_{CO,2}}{W_{CO}} + \left(\frac{Y_{CO,1}}{W_{CO}} - \frac{Y_{CO,2}}{W_{CO}}\right) Z_{st} + \frac{Y_{F,1}}{W_F} Z_{st}\right]$$
$$Y_{H2O,st} = W_{H2O}\left[2\frac{Y_{F,1}}{W_F} Z_{st}\right] \qquad (2.50)$$
$$Y_{N2,st} = 1 - Y_{CO2,st} - Y_{H2O,st}$$

The initial guess of c_p obtained from equation (2.45) is then iteratively improved by

$$c_{p,mix} = \frac{\int_{T_u}^{T_{st}} \left(Y_{CO2,st} c_{p,CO2} + Y_{H2O,st} c_{p,H2O} + Y_{N2,st} c_{p,N2}\right) dT}{T_{st} - T_u} \qquad (2.51)$$

giving an averaged $c_{p,mix}$ over the temperature range for set mass fractions of the components. The results indicate that the average $c_{p,mix}$ of the mixture cannot be assumed to be constant especially when carbon monoxide is added on the oxidizer side.

$Y_{CO,1/2}$	CO addition on Air Side $c_{p,mix}$ @ $T_{ad,2000K}$	CO addition on Air Side $c_{p,mix}$ @ $T_{ad,2100K}$	CO addition on Fuel Side $c_{p,mix}$ @ $T_{ad,2000K}$	CO addition on Fuel Side $c_{p,mix}$ @ $T_{ad,2100K}$
0,000	1304	1322	1304	1322
0,010	1299	1316	1304	1321
0,020	1293	1311	1303	1321
0,030	1288	1306	1303	1321
0,040	1283	1300	1303	1321
0,050	1278	1295	1302	1320
0,060	1272	1290	1302	1320
0,070	1267	1284	1302	1320
0,080	1262	1279	1301	1319
0,090	1257	1273	1301	1319
0,100	1251	1268	1301	1319
0,110	1246	1263	1301	1318
0,120	1241	1257	1300	1318
0,130	1236	1252	1300	1318

0,140	1230	1246	1300	1317
0,150	1225	1241	1299	1317
0,160	1220	1236	1299	1317
0,170	1215	1230	1299	1316
0,180	1209	1225	1298	-
0,190	1204	1220	1298	-
0,200	1199	1214	1298	-
0,210	1194	1209	1297	-
0,220	-	1203	1297	-
0,230	-	-	1297	-
0,240	-	-	1297	-

Table 2.5: Variable average $c_{p,mix}$ for the two different Adiabatic Flame Temperatures and CO addition on both Fuel and Air Side. $c_{p,mix}$=J/kg*K.

Table 2.5 doesn't provide values for every $c_{p,mix}$ up to CO mass fractions of 0.24 since this partially led to negative mass fractions which is practically not feasible. Those values were truncated.

The c_p for the product species CO_2, H_2O, N_2 were calculated by refering to the NASA polynomials

$$c_p = R(a_1T^{-2} + a_2T^{-1} + a_3 + a_4T + a_5T^2 + a_6T^3 + a_7T^4) \quad (2.52)$$

with the gas constant $R = 8{,}31451\frac{J}{mol*K}$.

Coefficient	CO_2	H_2O	N_2
a_1	4,943650540E+04	-3,947960830E+04	2,210371497E+04
a_2	-6,264116010E+02	5,755731020E+02	-3,818461820E+02
a_3	5,301725240E+00	9,317826530E-01	6,082738360E+00
a_4	2,503813816E-03	7,222712860E-03	-8,530914410E-03
a_5	-2,127308728E-07	-7,342557370E-06	1,384646189E-05
a_6	-7,689988780E-10	4,955043490E-09	-9,625793620E-09
a_7	2,849677801E-13	-1,336933246E-12	2,519705809E-12

Table 2.6: NASA Coefficients for calculating thermal properties of CO_2, H_2O, N_2 for a temperature range from 200K to 1000K. [11]

Due to reasons of mathematic accuracy of this approach the coefficients usually change at a temperature of 1000K. This change is not only necessary for the calculation of c_p but also for that of Enthalpy H and Entropy S.

Coefficient	CO_2	H_2O	N_2
a_1	1,176962419E+05	1,034972096E+06	5,877124060E+05
a_2	-1,788791477E+03	-2,412698562E+03	-2,239249073E+03
a_3	8,291523190E+00	4,646110780E+00	6,066949220E+00
a_4	-9,223156780E-05	2,291998307E-03	-6,139685500E-04
a_5	4,863676880E-09	-6,836830480E-07	1,491806679E-07
a_6	-1,891053312E-12	9,426468930E-11	-1,923105485E-11
a_7	6,330036590E-16	-4,822380530E-15	1,061954386E-15

Table 2.7: NASA Coefficients for calculating thermal properties of CO_2, H_2O, N_2 for a temperature range from 1000K to 6000K. [11]

3 Experimental Setup

The experiments were conducted at ambient pressure (1 atm) and ambient temperature (298K). The necessary air on the oxidizer side was provided by locally compressed and dried air which was found to offer a very accurate level of oxygen compared to bottled air according to previous experiments. The amount of lubricant in the dried air remains on a negligible level and the oxygen mole fraction of 0.21 proofs to be constant with little fluctuation compared to compressed air in bottled containers. Both the methane and nitrogen in use offered minimum purity levels of 99% to provide sufficient accuracy throughout the experimental part of the research.

Carbon Monoxide posed a very critical aspect on the experiment especially considering its hazardous capability. The piping containing CO was completely substituted by stainless steel piping to bar the risk of having material hardening, eventually leading to brittle plastic and leakage in the system. Moreover the system had to be extensively tested on leakages and other possible defects. To ensure the identification of CO spills at the flame level itself two CO detection tools were put in place, set to a lower detection level of 20ppm.

The experiments itself were conducted on a counterflow setup with two opposing burner parts. The upper part was designed newly for the purposes of this experiment.

System control was realized through LabView and a specially designed GUI to direct the mass flow controllers as well as their calibration and the temperature sensing units.

3.1 Chemical Components

For calculation purposes the used compressed air was reduced to its two major chemical components Nitrogen N_2 and Oxygen O_2. In combination with the reactants methane CH_4 and carbon monoxide CO and by applying the principles of one step chemistry and complete combustion the chemical reaction

$$\mathbf{CH_4 + 2CO + 3O_2 + a_{N_2}N_2 \rightarrow 3CO_2 + 2H_2O + a_{N_2}N_2}$$

will form the products Water H_2O, Carbon Dioxide CO_2 and Nitrogen N_2.

Table 3.1 is showing the chemical components' material properties relevant to the calculation presented in *2. Experimental Parameters*.

Chemical Component	Mean Molecular Weight [g/mol]	Heat of Formation at 298K [kJ/mol]	Latent Heat at 2000K [kJ/mol]	Latent Heat at 2100K [kJ/mol]
	$\bar{M}_n$	ΔH_f°	$H^\circ(2000\mathrm{K}) - H^\circ(298\mathrm{K})$	$H^\circ(2100K) - H^\circ(298K)$
CH_4	16,04276	-74,873	123,592	133,087
CO	28,0104	-110,527	56,744	60,376
N_2	28,0134	0	56,137	59,742
O_2	31,9988	0	59,175	62,961
H_2O	18,01528	-241,826	72,79	77,941
CO_2	44,0098	-393,522	91,439	97,488

Table 3.1: Material properties of the molecules given in the basic, one-step chemical reaction and CO. [12]

3.2 Experimental Apparatus

3.2.1 Mass Flow Control

The mass flows of the up to seven streams are controlled by seven independently working Teledyne Hastings Instruments mass flow controllers. Throughout the experiment two different types were used: HFC-302 and HFC-303. They ranged from theoretically maximum flows of 5 SLM (HFC-302), 10 SLM (HFC-302), 30 SLM (HFC-303), 50 SLM (HFC-303) up to 100 SLM (HFC-303). SLM hereby stands for Standard-Liters-Per-Minute. Standard-Liters-Per-Minute denominates the volumetric flow normalized to ambient pressure and room temperature.

The Mass Flow Meter itself consists of a base, a shunt, a control valve, the electronic circuitry and a sensor that is able to measure gas flow rates from 25-10.000 SLM. The shunt divides the overall gas flow in two laminar flows, where the flow through the sensor is a precise fraction of the total flow through the shunt. The control valve adjusts the flow so that the sensor's measurement matches the setpoint input. The circuit board amplifies the sensor output from the two resistive temperature detectors (RTD) and provides an analog output of either 0 - 5 VDC or 4 - 20 mA.

Figure 3.1: The left side of the picture is showing the Mass Flow Controllers (Teledyne HFC-303) used to guarantee defined mass fractions of the streams. The right side of the picture depicts a Ritter TG 5/5-ER – Drum-type Gas Meter, suitable for minimum flow rates of 10ltr/h up to maximum flow rates of 2000ltr/h and used for calibration of the MFCs.

Every Mass Flow Controller has to be set up for the type of gas it controlled. Based on the computational models and predicted extinction strain rates the MFCs were calibrated to the expected range of use. The tool to guarantee accurate calibration was the Ritter TG 5/5-ER – Drum-type Gas Meter. It measures the volumetric flow of a gas volume by the principle of positive

displacement. The entering gas causes a rotation of the measuring drum, constantly filling and emptying a rigid measuring chamber.

The calibration instrument was connected to the PC and the data read-out digitally. For each gas and each Mass Flow Controller 5 flow rates in the relevant sector got selected and each of them measured for at least 3 times. Necessary adaptations were implemented by either adapting the maximum flow rate for the gas respectively shifting the zero point of the linear function.

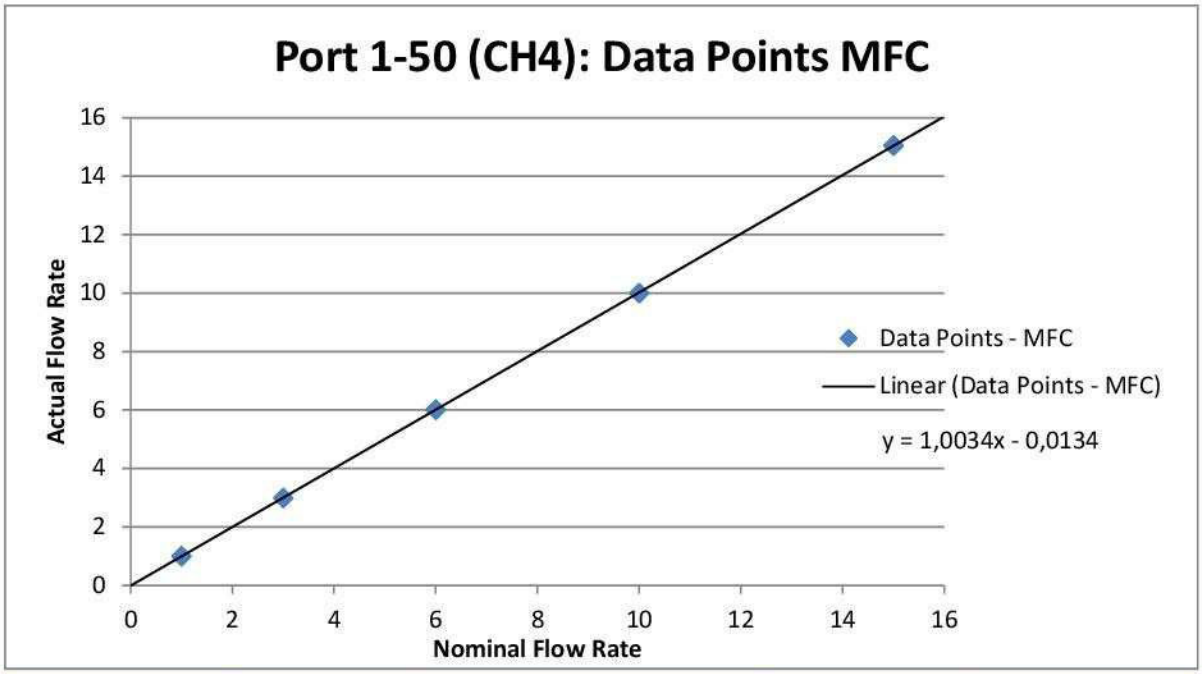

Nominal Flow Rate	Actual Flow Rate	Max Flow Rate	Suggested Max Flow Rate	Deviation	Number of Data Points
1	1,001	41,1	41,1	0,10%	3
3	2,99	41,1	40,96	-0,33%	4
6	6,01	41,1	40,97	0,17%	3
10	10	41,1	41,1	0,00%	4
15	15,05	41,1	41,19	0,33%	3

Figure 3.2: Exemplary test record for the calibration of methane. The used MFC had a range of 50SLM whereat only the range of up to 18SLM was relevant to this experiment.

The Ritter Gas Meter offered a ± 0.5% accuracy over full measurement range. The calibration certificate to the Ritter Gas Meter can be found in **Fehler! Verweisquelle konnte nicht gefunden werden. Fehler! Verweisquelle konnte nicht gefunden werden.**.

3.2.2 Temperature Measurement

The temperature in the flame zone is being monitored by employing a thermocouple right in between the upper and lower part of the counterflow burner. Thermoelectric Effect Sensors (=Thermocouples) rely on the physical principle of two different metals connected together that adhere to a function dependent on the temperature and generated at the junction between the metals. Thermocouples can be manufactured from a wide variety of materials; in this case a type R thermocouple was used. Platinum thermocouples (type R) have one wire made from pure platinum and the other wire made from a platinum-rhodium alloy with 13% rhodium. Their quoted measuring range is 0 to +1700°C, with a measurement sensitivity of 10 µV/°C and a quoted inaccuracy of ±0.5%. [13]

The wires both measuring 0,076 mm in diameter add up to a diameter of 0,21 mm at the bead of the welding. To avoid short-circuiting the two conductors are separately routed through a ceramic tube to the plug of the thermocouple.

Figure 3.3.: Thermocouple Type R, Platinum/13%-Rhodium-Platinum

The sensor is placed on a 3-dimensional-moveable mounting to get it in the required position. By assuring that the thermocouple respectively the sensor wires are placed orthogonal to the flow (to prevent from heat conduction along the wire) accurate measurements of the gaseous flow temperatures can be expected. The temperature profile close to the duct exit proofed to be near to constant both in the direction of its radial and axial axis. Also the bending of the bead wire occurring under high strain rates proofed to have little influence on the accuracy of the measurements. [7]

The initially measured temperature has to be corrected by the influence of the thermocouple on the flame temperature according to the equation

$$T_c = T_{tc} + \frac{\varepsilon \sigma d T_{tc}^4}{2\lambda} A \qquad (3.1)$$

where T_c is the corrected gas temperature, T_{tc} is the initially indicated temperature by the thermocouple, ε the emissivity, σ the Boltzmann Constant, d the diameter of the bead, λ the thermal conductivity of the bead material and A the view factor, assumed to be 0,5 since it is only the lower part of the bead that can emit radiation. The emissivity ε is 0,128 following [14], the thermal conductivity λ is calculated in accordance with previous studies from [7] to

$$\lambda = 4{,}6942 * 10^{-3} + 8{,}1225 * 10^{-5} T_{tc} - 1{,}4547 * 10^{-8} T_{tc}^2 \qquad (3.2)$$

3.2.3 System Control

The program in use to control, calculate and set the mass flows is NI LABVIEW. LABVIEW, an acronym for Laboratory Virtual Instrument Engineering Workbench, uses the means of graphical programming by applying a dataflow model. The graphical programming language is called G and allows the user to model the structure of Virtual Instruments (VI). VIs hold the graphical block diagrams which are determining the routines. They can be modeled according to the user's needs an offer a lot of flexibility by connecting function nodes through creating wires in between them. VIs are independently executable and can easily be implemented in other VIs as sub-routines. The program routine is displayed to the end user through an User Interface (UI) offering a graphically appealing design.

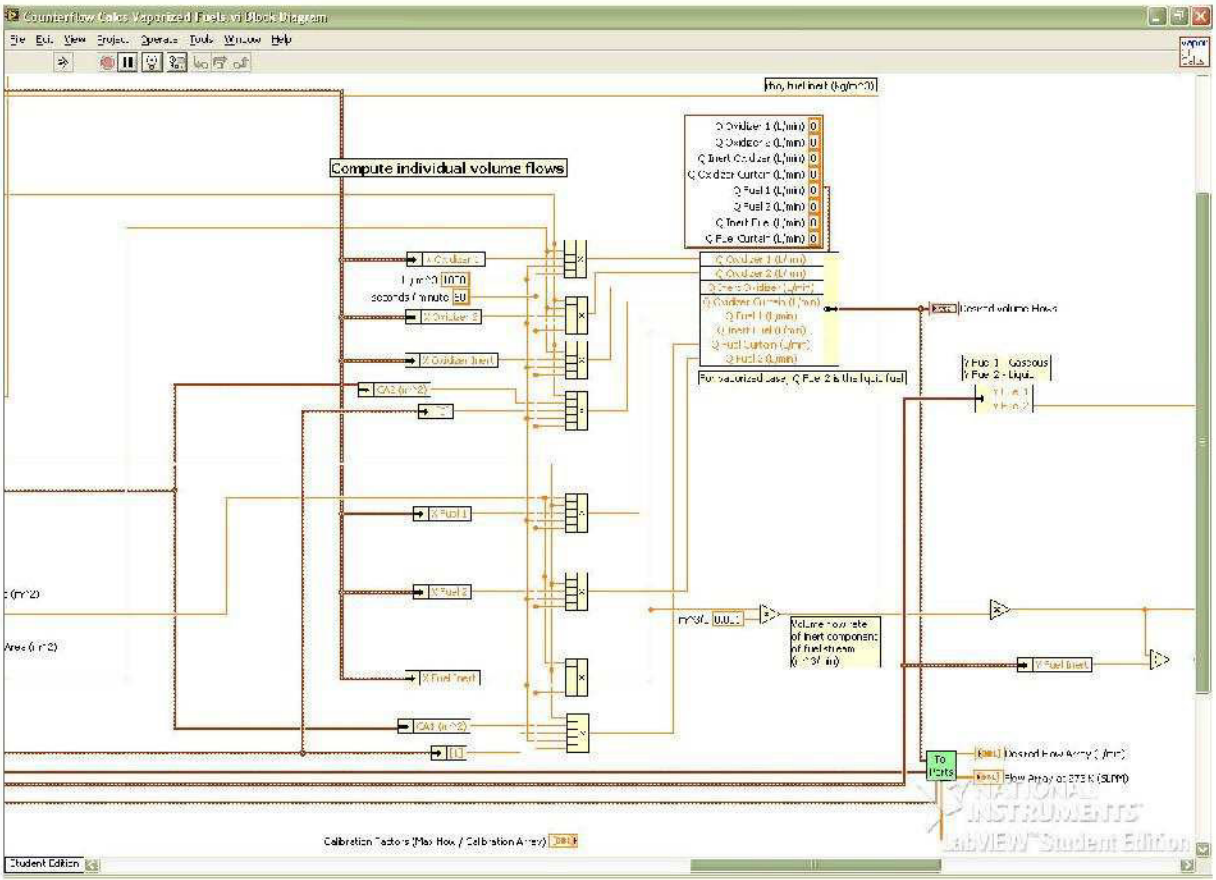

Figure 3.4: Detail of the main VI of the used routine to control and calculate the mass flows for the experiments.

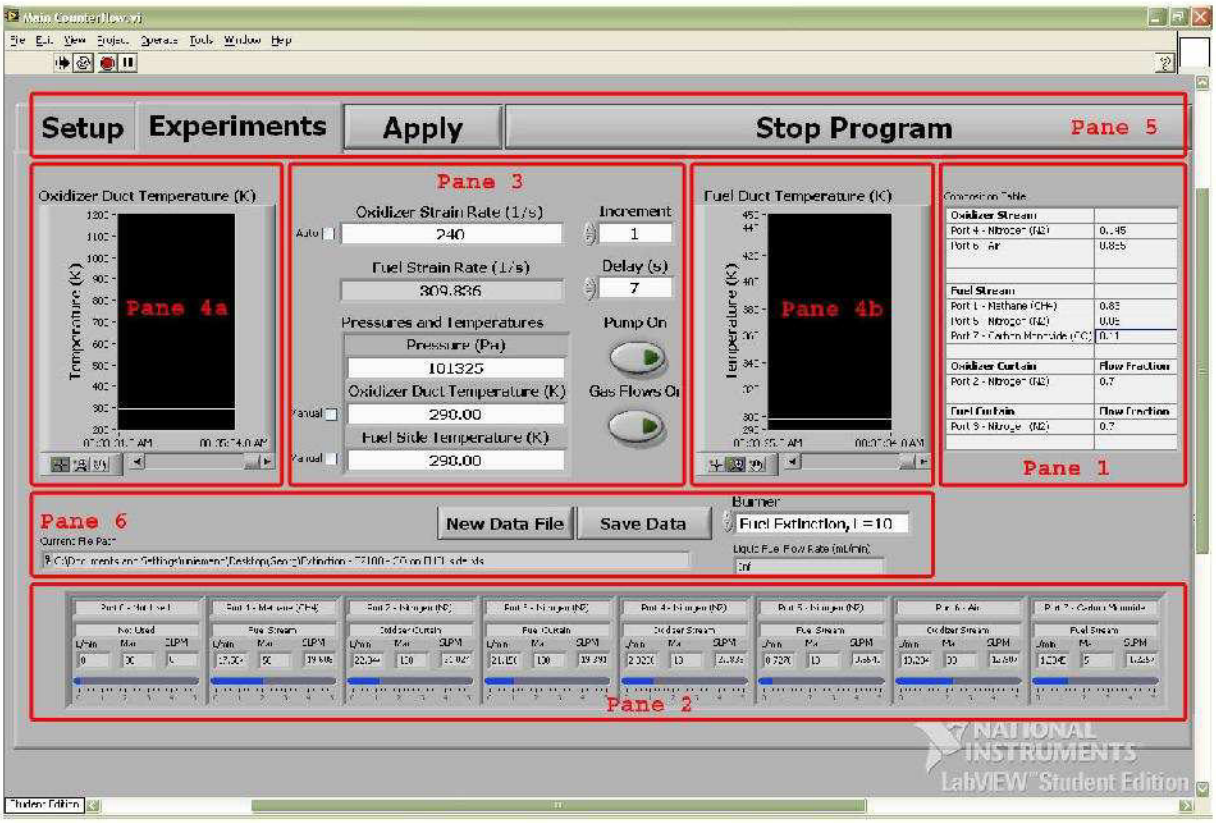

Figure 3.5: Main User Interface for the VIs in use consisting of 7 panes.

Figure 3.5 shows the main user interface which was in place to control the mass flows and set the variables necessary for the experiments.

Pane1: Shows the mass fractions of the Fuel Stream as well as the Oxidizer Stream. The appendant VI was programmed to automatically identify the inert gas(es) and calculate them for each stream to sum up to 1. All other mass fractions were set according to the calculated values. Assigning different gases to the Fuel respectively Oxidizer Streams and Curtains was done in another GUI.

Pane2: Offers an easy overview of the separate gas flows. Depending on the strain rate and the Mass Fractions it gives a good idea if the Mass Flow Controllers (MFC) are reaching its limits and drops a warning once that limit is reached. Since it's only a calculated, theoretical value and no factual response from the MFC system, the values on the digital controlling unit have to be checked upon as well. The real-time information if the gas flow is lower/higher than supposed to (i.e. due to an emptying gas bottle) can be easiest found there.

Figure 3.6: Two Teledyne PowerPods 400 supplying the MFCs with power. They are connected to LabView through a RS-232 cable connection enabling the user to control the MFCs.

Pane3: Is the input field to set the strain rate of the Oxidizer Stream and gives the strain rate of the Fuel Stream based on the underlying calculation and meeting the criteria of momentum balance of both streams. A critical point for both autoignition and extinction experiments with variable strain rates is to approach the point of ignition/extinction slowly. Therefore an automatic mechanism was implemented to raise the strain rate by a defined amount after a defined time elapsed. For the extinction experiment the increase in strain rate was set to 1 s^{-1} every 7 seconds. This empirically defined value gave the system sufficient time to attune to the change in strain rate and hence mass flows.

Pane 4: Two temperature charts display the temperature measured in the reaction zone and in the fuel stream before entering the lower part of the burner. Both of the temperature charts play an important role when carrying out autoignition experiments, especially with liquid fuels. Liquid fuels have to be vaporized before entering the reaction zone and get therefore heated up. The applied thermocouple in the fuel pipe helps controlling that process. The thermocouple in the reaction zone gives direct information on the temperature of the mixture and determines in combination with an optical system at which temperature the mixture ignites.

Pane5: Offers an emergency shut off, the tab to the main user interface and another tab to set up the allocation of the gases to the different streams. There, one can also find the connected sub-routine for calibrating each Mass Flow Controller based on the gas in use.

Pane6: Allows to save the obtained data and all connected, relevant information in a *.xls file.

3.2.4 Counterflow Burner

Fuel in form of CH_4 will only be added via the fuel side (=lower part, index 1), O_2 as Oxidizer will only be added through the air side (=upper Part, index 2) of the Burner. N_2 and CO can be added on either side depending on the required experimental setup.

Figure 3.7: Pictures of a stabilized flame in the counterflow burner. The mass fraction of CO $Y_{CO,O}$ in the oxidizer stream on the picture on the left side is $Y_{CO,O}$=0.14, the mass fraction of CO in the fuel stream on the right side is $Y_{CO,F}$=0.14. Both pictures were taken at the setup for an adiabatic flame temperature of T_{ad}=2000K and shortly before its respective extinction strain rate.

Via the two opposing ducts the fluxes of fuel, oxygen, nitrogen and the additive carbon monoxide are induced forming a stagnation layer by fulfilling the momentum balance of

$$\rho_1 * {V_1}^2 = \rho_2 * {V_2}^2 \tag{3.3}$$

Primarily depending on the composition of the mixture and the temperature the two fluxes reach a stoichiometric, combustible state near the stagnation plane and form a flame level.

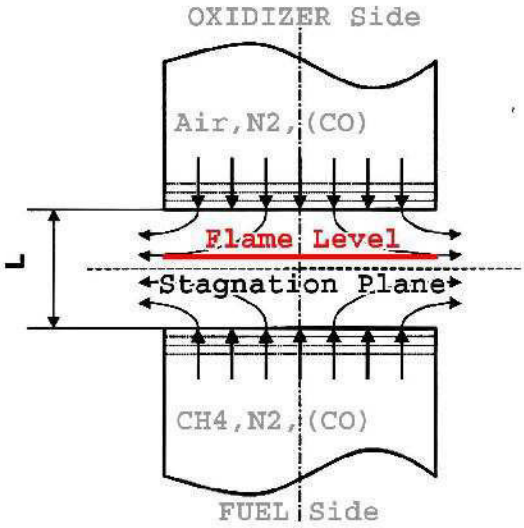

Figure 3.8: Schematic illustration of a laminar non-premixed counterflow diffusion flame. The stagnation plane is defined by the momentum balance of the two fluxes, the position of the flame by the diffusional processes.

The previous figure indicates the position of the flame level qualitatively. Generally can be said that its position will be closer to the oxidizer side if the number of moles oxygen per mole fuel for stoichiometric combustion is large, or the oxygen concentration in the oxidizer stream is small, or the fuel concentration in the fuel stream is large. [15]

3.2.4.1 Upper Part

The upper part of the burner, also called the oxidizer part, mainly consists of two concentric ducts and a stainless steel containment. The inner pipe directs the air flow respectively the air and carbon monoxide mixture towards the inner duct of the lower part of the burner supplying the fuel respectively the fuel and carbon monoxide mixture.

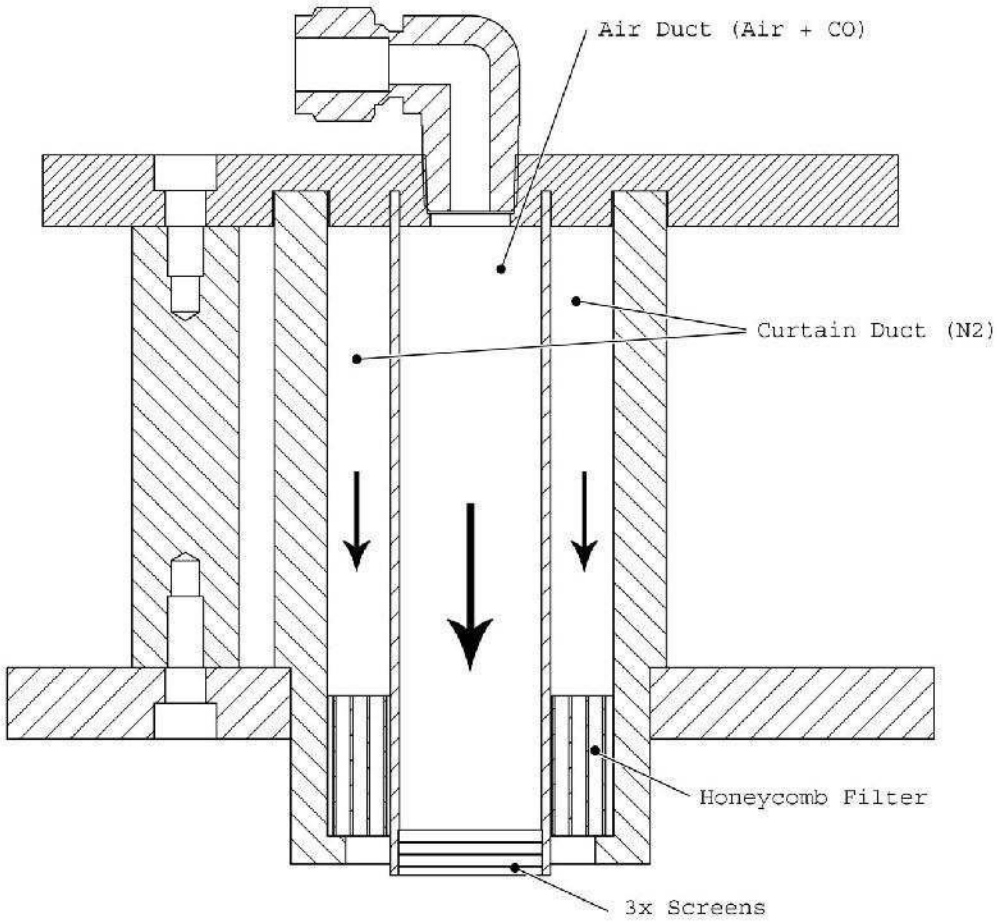

Figure 3.9: Schematic diagram of the working principle of the upper part of the extinction burner.

Three fine wired 200-meshes (200 meshes per inch) are placed at the end of the duct to induce a slight pressure gradient and guarantee plug flow conditions at the exit of the duct. The meshes are held in place by stainless steel rings. The effective diameter at the exit of the duct is 22,2 mm which equals to the inner diameter of the stainless steel rings.

The outer pipe guides the nitrogen to the reacting zone in between the lower and the upper part where it creates a NO-curtain to shield the upper flux from the surrounding air.

3.2.4.2 Lower Part

The lower part of the burner, also called fuel part, routes the fuel respectively a methane-carbon monoxide mixture towards the reaction zone. It consists very similarly to the upper part of two concentric pipes where the inner one contains the fuel mixture and the outer one the nitrogen which fulfills the same function as the one in the upper part: to create a contagion to shield the reaction zone. The inner pipe features three layers of meshes at the end of the duct to guarantee plug flow conditions. The diameter of the inner fuel duct is exactly the same size as the oxidizer duct of the upper part.

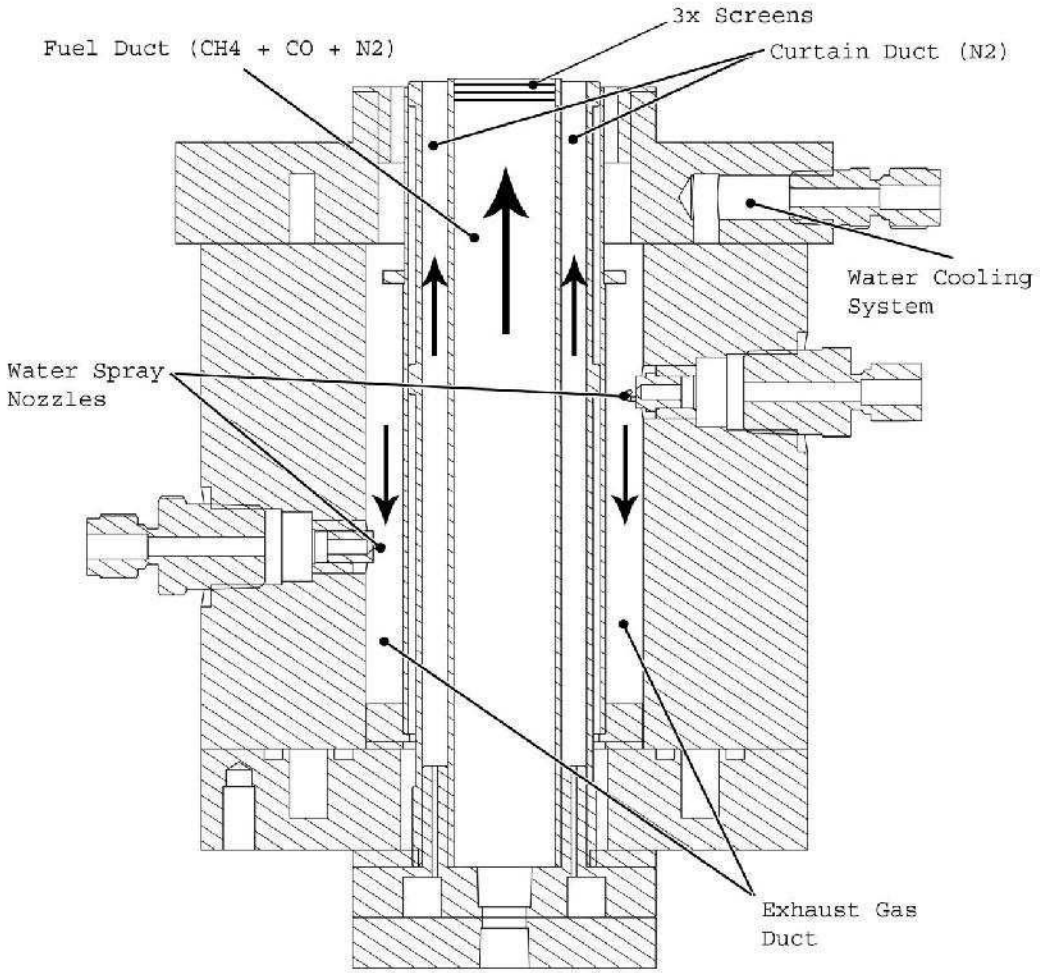

Figure 3.10: Schematic diagram of the working principle of the lower part of the extinction burner.

Another function of the lower part of the burner is the exhaust system. Mild suction is applied through a third concentric shaped opening around the fuel duct exit respectively the nitrogen curtain duct to keep exhaust gases from spreading uncontrolled.

The heated exhaust gases get cooled down by a water spray system inside the exhaust duct to keep the gases from further reacting. A special flange above the water nozzles is intended to keep water from interfering with the reaction zone.

4 Computational Simulation

Aside of experimentally researching chemical reactions of diffusion flames, the computational modeling and simulation of the same has become a standard nowadays. Reasons for that are on one side the evermore increasing processing power of CPUs and constantly improving accuracy of computational models. On the other side it's the simple fact that simulation compared to experimental work can usually be done easier, faster and at lower cost. Computational simulation other than experimental work is furthermore not restricted by physical limitations of the measuring equipment, enabling research in fields that are experimentally not possible.

The experimental work presented in this diploma thesis has been conducted together with a computational simulation using CHEMKIN Pro which allows the exact modeling of complex chemical proceedings.

The computational work itself was parallel carried out by a colleague, Mrs Vaishali Amin MSc.

4.1 CHEMKIN Pro

CHEMKIN is a modularly structured package of programs used to describe the reaction-kinetical behavior of reactions of different gas phases. Basically it consists of three different components:

- The Interpreter,
- a library of calculation routines for thermodynamical data and state variables of gas mixtures, and
- a number of applications through which repeatedly used reaction-kinetical models can be applied.

Reaction Mechanisms are the basis for describing chemical processes in CHEMKIN. Reaction Mechanisms can be understood as a compilation of elemental chemical reaction equations. Reaction Mechanisms describing the combustion behavior of hydrocarbons can be very comprehensive and consist of hundreds of chemical reaction equations. As a consequence of this possible complexity, there's a number of mechanisms that have been simplified by reducing the number of reaction equations. This reduction can lead to a significant drop in required processing power and hence processing time without substantially influencing the quality of the result. CHEMKIN is importing Reaction Mechanisms through its so called Interpreter in form of ASCII data. The CHEMKIN formatting of these files became widely used over time which lead to a large number of Mechanisms being readily available to be downloaded through websites and implemented. [16]

The Interpreter uses the reaction mechanism file together with the thermodynamical data file (containing polynomial coefficients for calculating caloric state variables like the enthalpy, entropy,

etc.) to create a binary file that can be used by CHEMKIN respectively its applications. Some CHEMKIN applications additionally require a transport data file containing e.g. diffusion coefficients.
The mechanism used in this calculation was the San Diego Mechanism as described in *4.2 The San Diego Mechanism*.
The library of calculation routines consists of a large number of FORTRAN sub-routines. Through them the properties of species, mixtures or species forming rates can be determined. Since they are FORTRAN sub-routines they can also be implemented in self compiled programs.
Besides the Interpreter and the library of calculation routines CHEMKIN offers a number of applications with which idealized model reactors can be simulated. The most relevant to this research was the CHEMKIN Reactor Model: Diffusion or Premixed Opposed-flow Flame and Premixed Burner-Stabilized Stagnation Flame.

4.2 The San Diego Mechanism

The San Diego Mechanism is the "reactional fundament" underlying the computational work being done by CHEMKIN. It was developed in over 10 years of work by the Combustion Research Group at UCSD and revised nearly every year after its initial launch in 2001.
As of 09/2012 it consists of 235 reaction equations providing the necessary information on calculating the reaction behavior of low-carbon fuels, including JP10 and Heptane.
The Research Group is describing the philosophy behind the mechanism as following:

The detailed chemistry is designed to focus on conditions relevant to flames, high temperature ignition and detonations. It was derived by beginning with simple chemical systems then proceeding gradually to more complex systems. In this approach, the numbers of species and reactions are kept to the minimum needed to describe the systems and phenomena addressed, thereby minimizing as much as possible the uncertainties in the rate parameters employed. The philosophy thus differs from that underlying a number of other data bases, many of which seek completeness, attempting to include all potentially relevant elementary steps.
In following the plan based on the present philosophy, the experience has been that the rate parameters of a relatively small number of elementary steps are of crucial importance to the predictions and that cumulative effects of small contributions from a large number of steps are seldom of much significance. This is advantageous because the many uncertainties in rate parameters of many steps increase the uncertainties in predictions when large number of steps are included. As the database for the present mechanism evolves, it should be applicable to an increasing number of combustion and detonation processes. [16]

4.3 Computational Setup

For the computational determination of the extinction strain rates when adding CO to a CH_4 flame at a fixed adiabatic flame temperature and a constant mixture fraction the following setup was made in CHEMKIN Pro.

All, the gas-kinetic mechanism, the thermodynamic and the gas transport data were obtained from the San Diego Mechanism. These three data files were connected with the general setup "Opposed-Flow Flame" as relevant for the counterflow setup.

To characterize the molecular transport of species, energy and momentum in the multi-component gaseous mixture velocities, (thermal) diffusion coefficients and thermal conductivities have to be evaluated. For the present constellation of the mixture and with the usage of the

San Diego Mechanism the "Mixture-averaged Transport" option proved to provide the most accurate results when solving for the Gas Energy Equation.

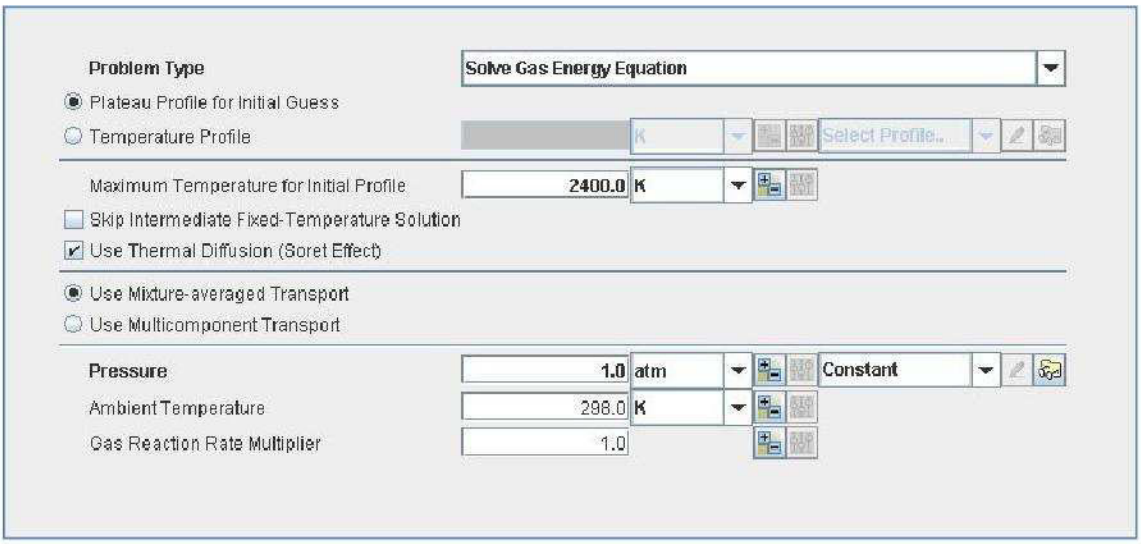

Figure 4.1: Setting of the reactor physical properties for Mixture-averaged Transport.

The number of uniform grid points was set to 700, with the further specifications:

- Adaptive Grid Control Based on Solution Gradient: 0.1
- Adaptive Grid Control Based on Solution Curvature: 0.5
- Maximum Number of Grid Points Allowed: 1000
- Number of Adaptive Grid Points: 5

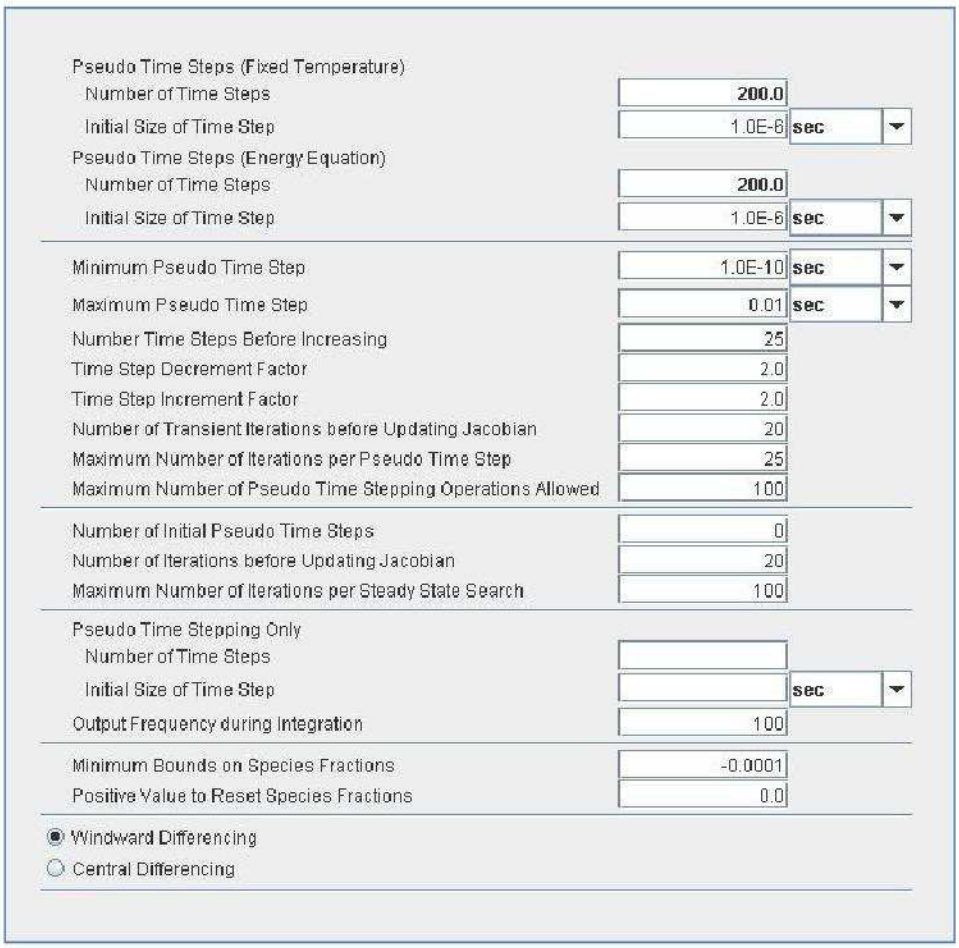

Figure 4.2: Mathematical Boundary Conditions for solving the Gas Energy Equations

In contrary to doing the practical experimental work the main parameter to change when doing the computational work was the duct velocity. For every single data point defined by its components' mass fractions a pre-defined list of duct velocities processed. The duct velocities of both the oxidizer and the fuel side hereby fulfilled the criteria of momentum balance.

By discretely increasing the duct velocities the diffusive behavior of the mixture changes and finally yields the desired results. The criterion that's checked upon hereby is the computed flame temperature which will – when reaching the extinction level – stay at the initial temperature of 298K along the whole flame region. The extinction duct velocities will after that be reversely calculated to show the extinction strain rates and compared to the experimentally collected extinction strain rates.

The computational work for this master's thesis was done by applying a manual approach in finding the extinction strain rate rather than using the automated approach in form of the arc-length continuation. [17]

The arc-length continuation is used to compute the solutions through the turning points. In theory, one can calculate the solutions up to the turning point using successive continuations on velocity. Such a technique requires smaller and smaller changes in the velocity, accompanied by more computational difficulty to get a solution, as the extinction point is approached. [18]

The reason for applying the manual approach which mainly differs to the arc-length continuation by manually choosing the boundary velocities of the oxidizer and fuel ducts was that the automated formulation wouldn't yield converging results. The computational setup is currently being adopted to yield converging results for the arc-length continuation as well. The results of this work won't be a part of this master's thesis since they are still to be compiled.

5 Experimental/Computational Results

The experiments for carbon monoxide addition were conducted on the same experimental apparatus as the hydrogen addition experiments except for the newly designed extinction top.

In contrary to the corresponding experiments with hydrogen addition to either the fuel or the oxidizer stream, the CO-addition yielded different results. The hydrogen-methane mixture showed insensitiveness towards the location of hydrogen addition as can be seen in *Figure 5.1*. [1]

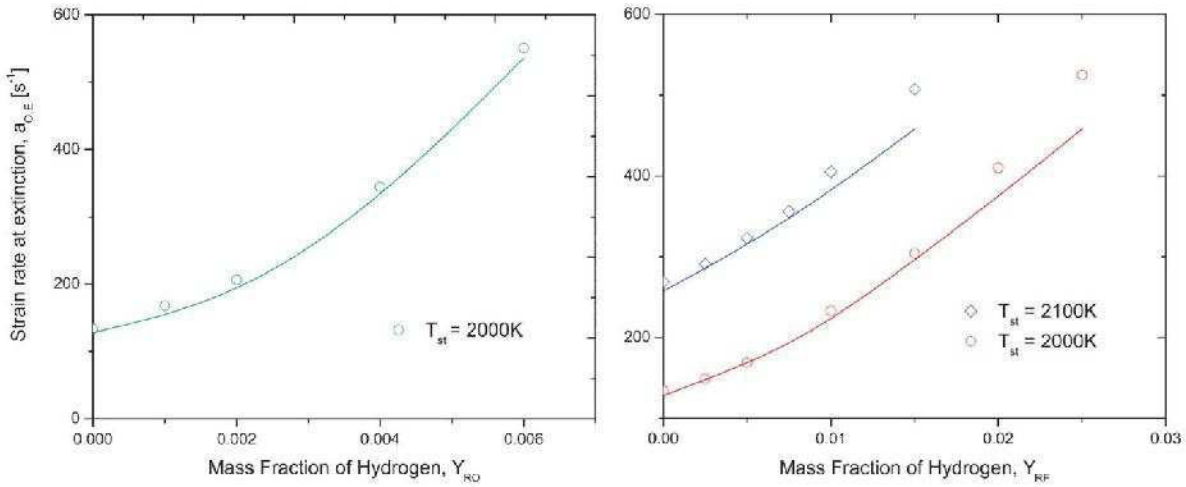

Figure 5.1: The oxidizer strain rate at extinction $a_{O,E}$ as a function of mass fraction of hydrogen in the oxidizer stream, Y_{RO}, respectively as a function of mass fraction of hydrogen in the fuel stream, Y_{RF}, at fixed Z_{st}=0.055 and T_{ad}=T_{st}=2000K and T_{ad}=T_{st}=2100K. The symbols represent experimental data and the curve represents predictions obtained using the San Diego Mechanism. [19], [20]

Not dependent on the side of the hydrogen addition, the oxidizer extinction strain rate increases in both cases with increasing fuel hydrogen mass fractions and oxidizer hydrogen mass fractions. Adding carbon monoxide instead of hydrogen as an additional reactant to a methane flame results in different behavior depending on which side carbon monoxide is added.

As can be seen in *Figure 3.7* and experimentally proven by the data in *Figure 5.2*, the position where carbon monoxide is added to a methane flame matters considering the change in extinction strain rate. Similar results can be found for CO addition at an adiabatic flame temperature of $T_{ad} = 2100K$.

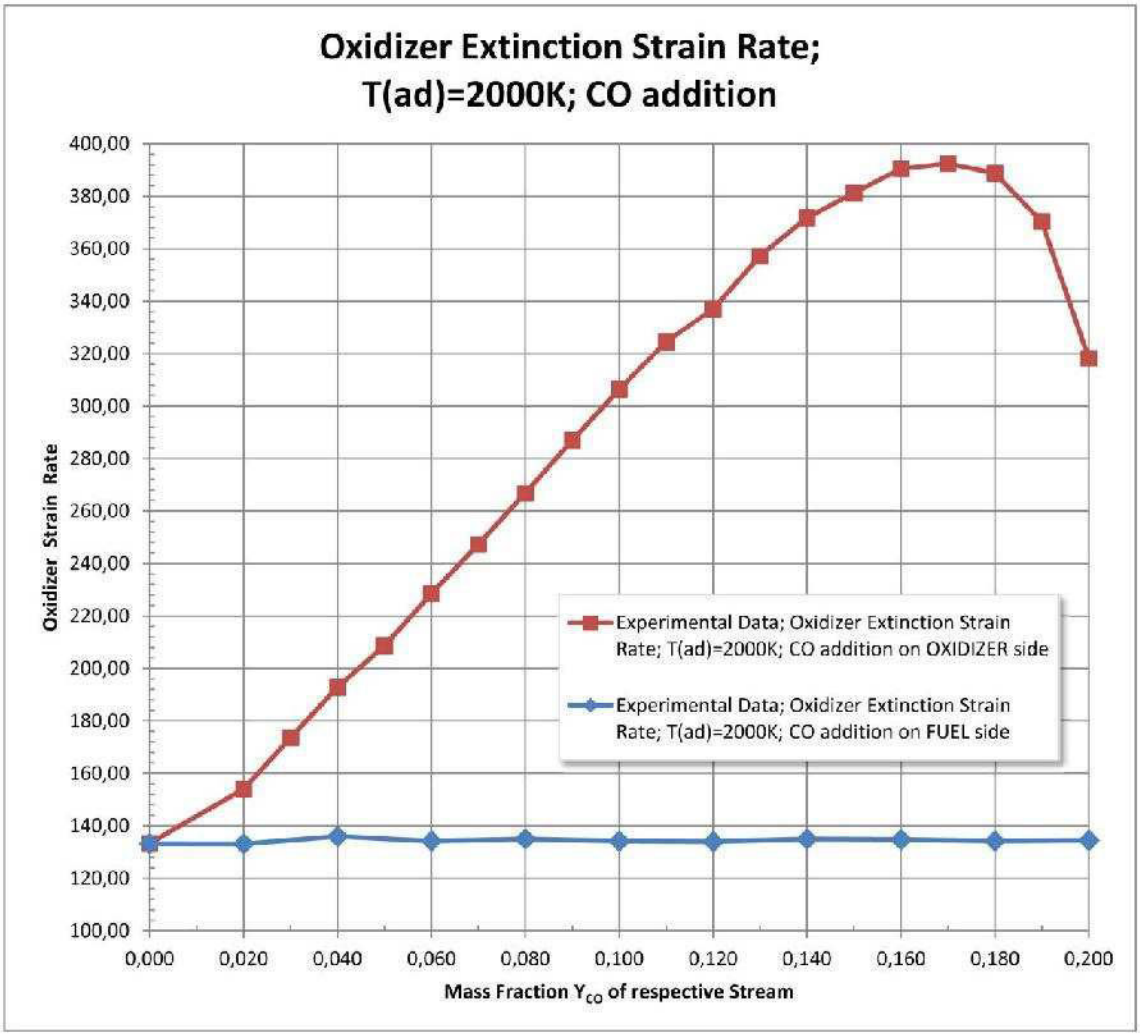

Figure 5.2: Oxidizer extinction strain rates as a function of the carbon monoxide mass fraction Y_{CO} at constant Z_{st}=0.055 and T_{ad}=2000K.

The carbon monoxide addition on the oxidizer side leads to an increase in strain rate, also resulting in a brighter, more intense combustion flame. The extinction strain rate of carbon monoxide addition on the oxidizer side experimentally peaks out at a carbon monoxide mass fraction of $Y_{CO,O} = 0.17$ showing a steep increase until that point and receding after that. For carbon monoxide addition on the fuel side on the other hand the extinction strain rate stays constant independent of the changing $Y_{CO,F}$.

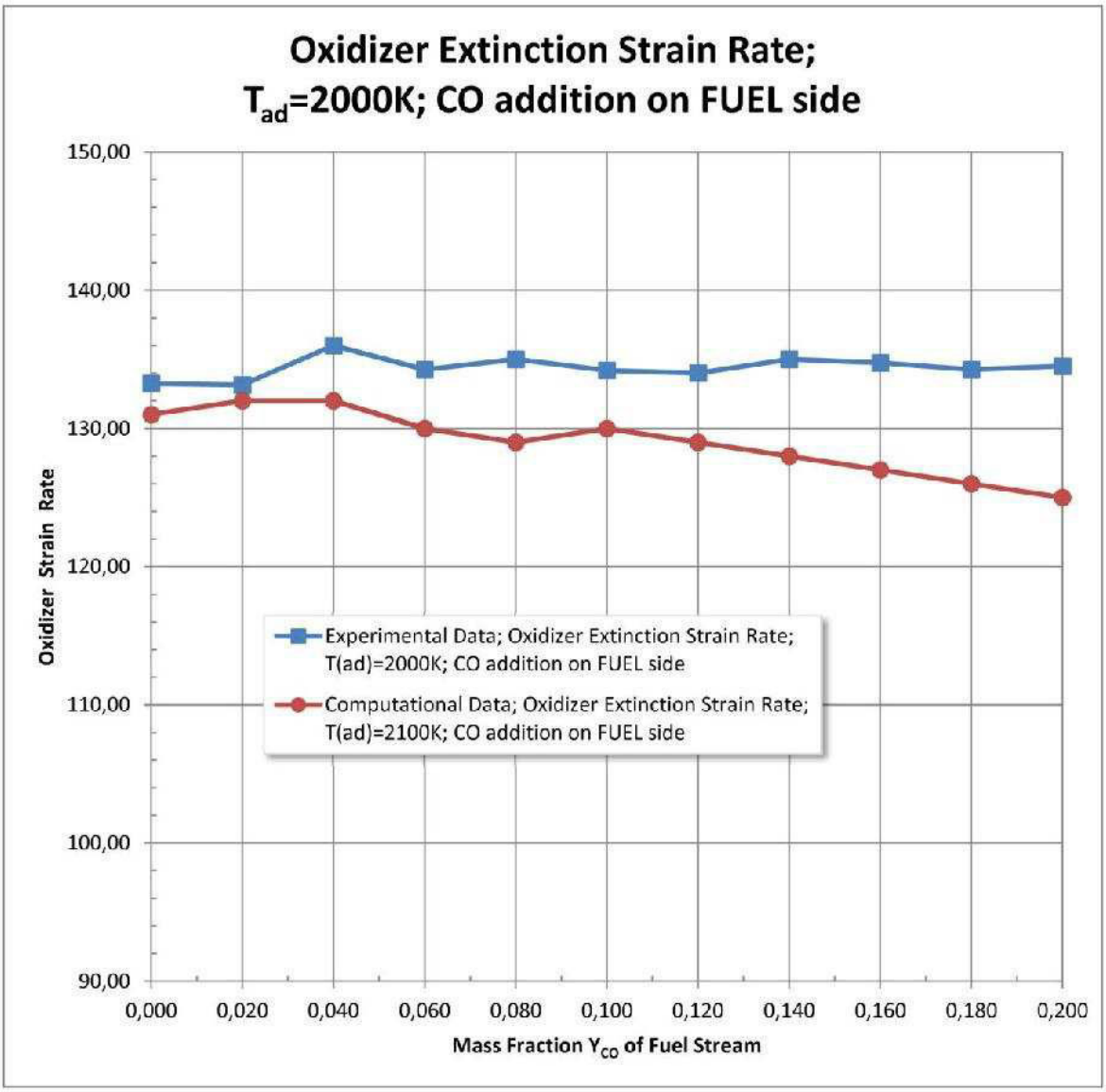

Figure 5.3: Oxidizer Extinction strain rate at constant T_{ad}=2000K and Z_{st}=0.055 and carbon monoxide addition in the fuel stream. The blue values show the experimental data, the red values the computational data obtained from CHEMKIN.

The computational simulation for an adiabatic flame temperature of $T_{ad} = 2000K$ and CO addition on the fuel side is in good agreement with the experimental data. Up to a CO mass fraction of $Y_{CO} = 0.10$ the experimental and the computational data show parallel behavior with an average absolute offset of 5 in strain rate. With increasing CO mass fraction the computational model indicates slightly receding oxidizer extinction strain rates whereas the experimental data remains at a constant oxidizer extinction strain rate of an averaged $a_{E,O} = 135s^{-1}$.

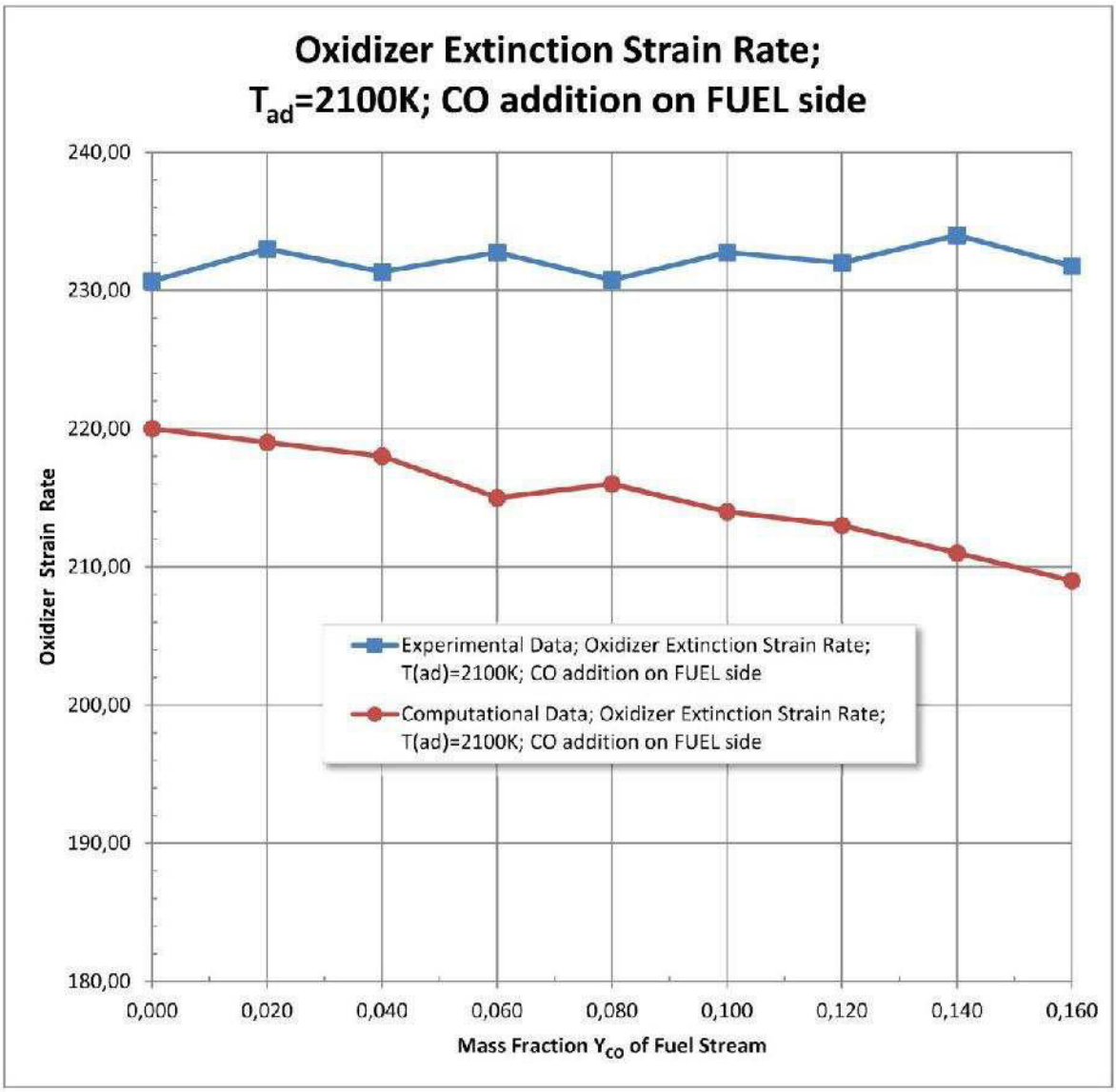

Figure 5.4: Oxidizer Extinction strain rate at constant T_{ad}=2100K and Z_{st}=0.055and carbon monoxide addition in the fuel stream. The blue values show the experimental data, the red values the computational data obtained from CHEMKIN.

The computational results for an adiabatic flame temperature $\mathrm{T_{ad}} = 2100\mathrm{K}$ and CO addition in the fuel stream also supported the data from the experimental work. The absolute difference at a CO mass fraction of $Y_{CO,F}$ increases from an absolute difference in between the experimental and the computational strain rate of 11 to 23 by computationally under predicting the experimental extinction strain rate. The trend of the experimental data is hereby slightly decreasing compared to a constant extinction strain rate obtained from the experimental data. This leads to a widening gap but is still of tolerable magnitude.

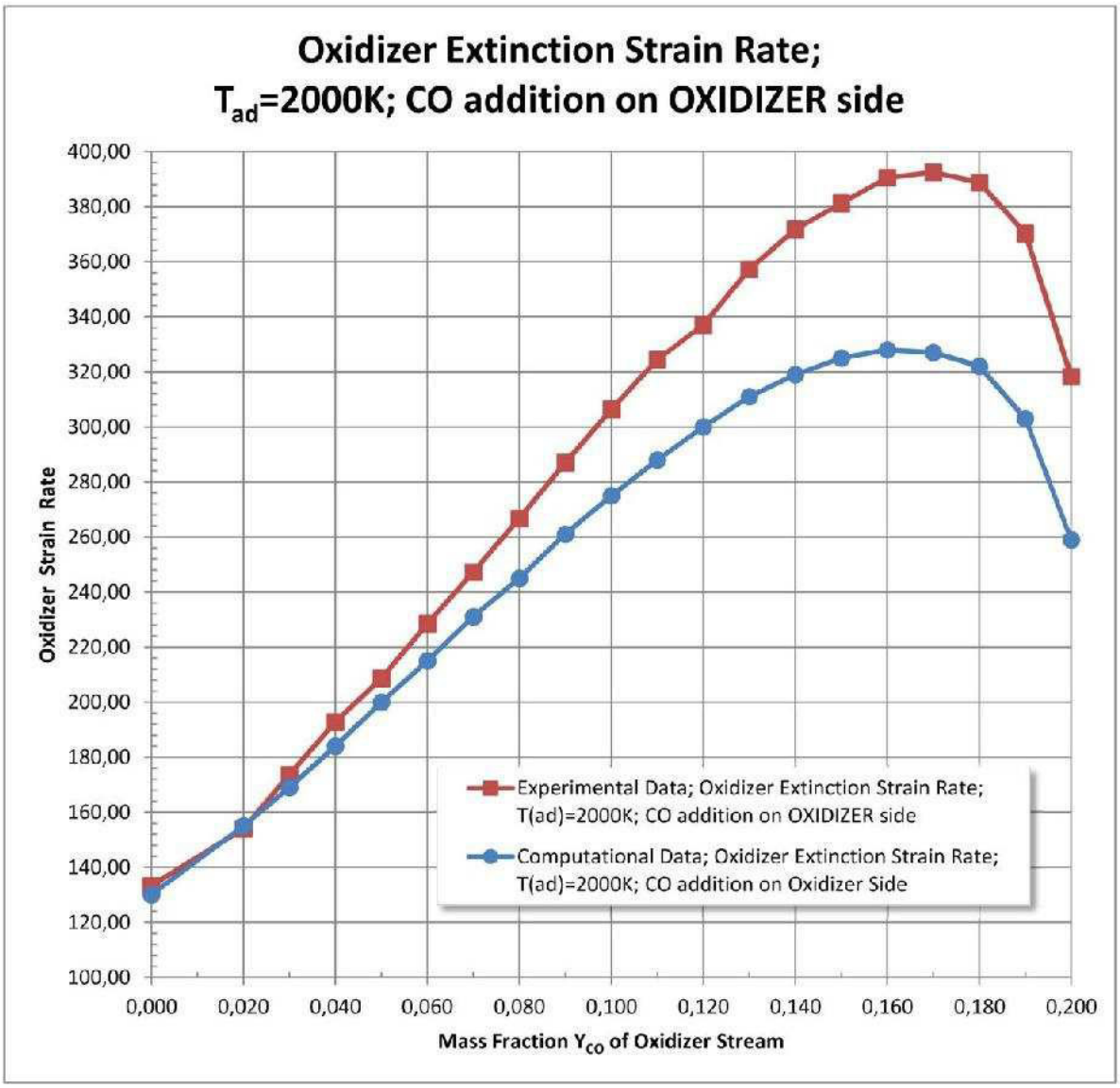

Figure 5.5: Oxidizer Extinction strain rate at constant T_{ad}=2000K and Z_{st}=0.055 and carbon monoxide addition in the oxidizer stream. The blue values show the experimental data, the red values the computational data obtained from CHEMKIN.

Unlike the oxidizer extinction strain rate for CO addition in the oxidizer stream, the oxidizer extinction strain rate for CO addition in the fuel stream shows a strong dependency on the CO mass fraction $Y_{CO,O}$. When looking at the case of an adiabatic flame temperature $T_{ad} = 2000K$ as shown in *Figure 5.5* a very clear peak can be defined at a CO mass fraction $Y_{CO,O} = 0.17$. After that the oxidizer extinction strain rate starts receding quickly. The computational data confirms this trend with a minor difference in the peak point ($Y_{CO,O} = 0.16$). The absolute values of the computational data clearly under predict the ones obtained from the experimental work with an absolute divergence of up to $\Delta a_{O,E} = 67s^{-1}$ at $Y_{CO,O} = 0.19$.

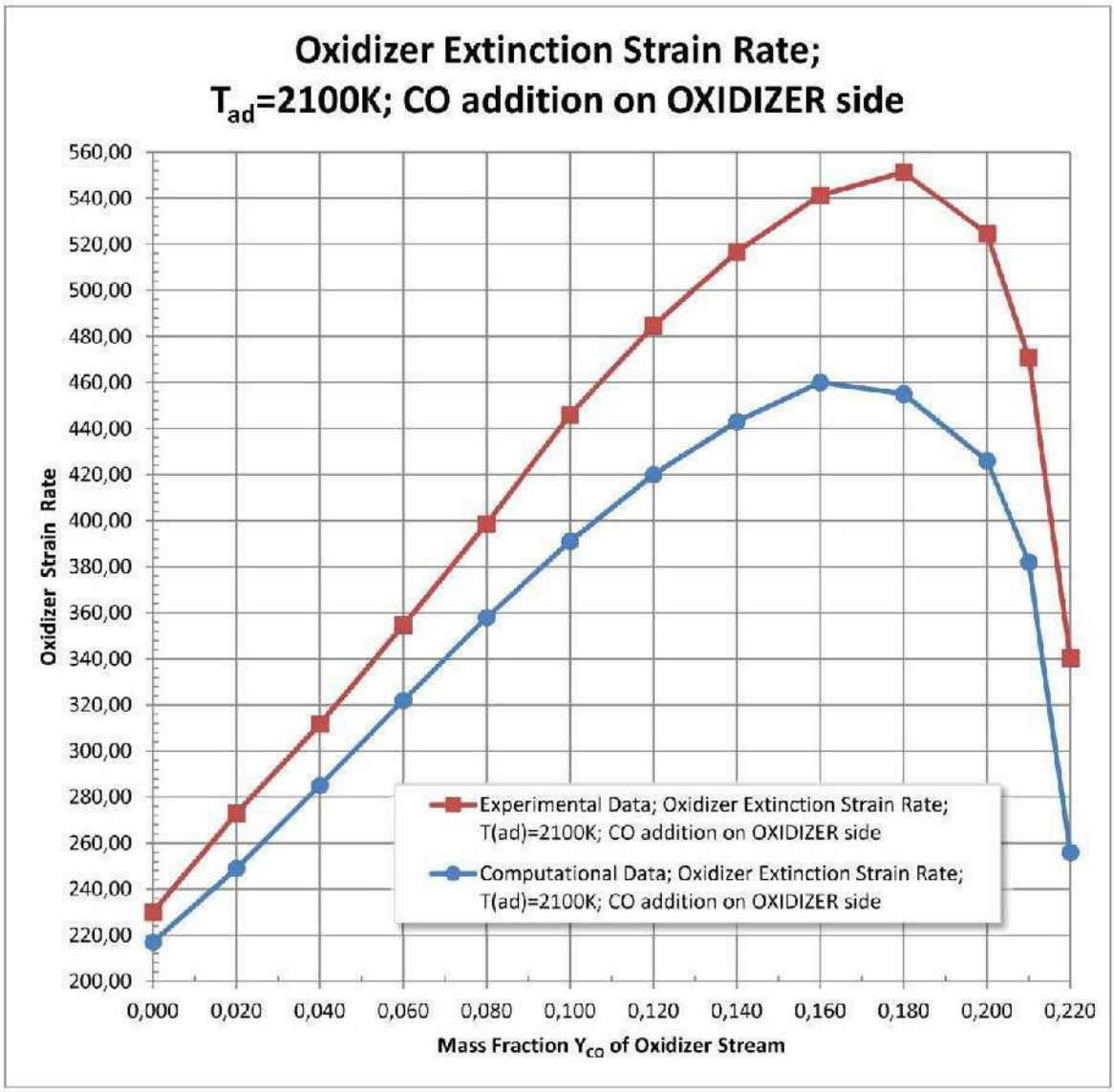

Figure 5.6: Oxidizer Extinction strain rate at constant T_{ad}=2100K and Z_{st}=0.055 and carbon monoxide addition in the oxidizer stream. The blue values show the experimental data, the red values the computational data obtained from CHEMKIN.

The experimental as well as the computational data for CO addition on the oxidizer side at a constant adiabatic flame temperature $T_{ad} = 2100K$ show trend wise similar results as those at $T_{ad} = 2000K$. The peak of the experimental oxidizer extinction strain rate can be found at $Y_{CO,O} = 0.18$ this time, that of the computational oxidizer extinction strain rate at $Y_{CO,O} = 0.16$. After that, both the data shows a steep receding behavior. Compared to the data at $T_{ad} = 2000K$ the oxidizer extinction strain rates yield much higher values which is due to the higher enthalpy because of the higher adiabatic flame temperature. The absolute values of the computational data clearly under predict the one obtained from the experimental work with an absolute divergence of up to $\Delta a_{E,O} = 99s^{-1}$ at $Y_{CO,O} = 0.2$.

6 Discussion

The data presented in this research shows very interesting results. It was not expected that the extinction behavior at a fixed adiabatic flame temperature and a constant mixture fraction would change that significantly when adding it to the fuel or the oxidizer stream. The results hereby show a very similar behavior at both fixed adiabatic flame temperatures of $T_{ad} = 2000K$ and $T_{ad} = 2100K$.

Furthermore it was not expected that the carbon monoxide addition on the fuel side would lead to such a pronounced peak at $Y_{CO,O} = 0.17$ for $T_{ad} = 2000K$ and at $Y_{CO,O} = 0.16$ for $T_{ad} = 2100K$. After peaking the oxidizer extinction strain rate shows a strong receding tendency for both cases up to its maximum mass fractions of $Y_{CO,O} = 0.19$ at $T_{ad} = 2000K$ and $Y_{CO,O} = 0.22$ at $T_{ad} = 2100K$.

This behavior is in clear contrast to the corresponding research with hydrogen addition which presented constantly increasing strain rates with increased mass fraction of hydrogen at the same fixed adiabatic flame temperatures. The detailed reasons for the extinction behavior of the methane-carbon monoxide mixture are currently being investigated and are not available at this point. With the use of CHEMKIN Pro, species profiles can be extracted for significant mixture points and evaluated. This should give a better understanding for the chemical kinetics during the combustion respectively give reasons for the differing behavior.

The computational model in general proves the experimental data. It tends to under predict the experimentally measured strain rates. The difference becomes significantly bigger at higher strain rates respectively higher mass fractions of carbon monoxide Y_{CO}. At an adiabatic flame temperature $T_{ad} = 2000K$ this can be an absolute divergence of up to $\Delta a_{O,E} = 67s^{-1}$ at $Y_{CO,O} = 0.19$, at an adiabatic flame temperature $T_{ad} = 2100K$ up to $\Delta a_{E,O} = 99s^{-1}$ at $Y_{CO,O} = 0.2$.
Despite the absolute differences between the computationally predicted and experimentally measured extinction strain rates, the computational results confirm the experimentally determined values by trend and can thus be used for comparison.

The computational model, especially the arc-length continuation is furthermore still being worked upon to give converging results. First, temporary results indicate the validity of the manual computational approach as well as the experimental data.

The present results clearly help to further the understanding of producer gas combustion. After researching the methane-flame behavior under hydrogen addition, the research on carbon monoxide addition was the next logical step. This knowledge can be expanded by examining the extinction behavior of a methane-flame under hydrogen and carbon monoxide addition on both the fuel and air

side by varying mass fractions. Adding both hydrogen and carbon monoxide to a methane flame would imitate a producer gas very closely and combined with the results obtained by this experiment and the hydrogen-addition, offer a holistic and comprehensive research in the field of producer gas in a counterflow setup.

The practical impact of those results is a significantly better understanding of producer gas combustion. Knowing that carbon monoxide can severely influence the quality of the combustion by varying its mass fraction and the point of addition will help to improve combustible processes.

7 Conclusion

The research was conducted on a counterflow apparatus in which two opposing, well balanced streams, one being the fuel flux, the other one the oxidizer flux, created a stagnation plane at which the stoichiometric conditions enabled the mixture to keep a stable flame.

Carbon monoxide was separately added to either the fuel or the oxidizer stream. The parameters stoichiometric mixture fraction Z_{st} and adiabatic flame temperature T_{ad} were hereby kept constant. The determining variable was the mass fraction of CO Y_{CO}. The resulting variable was the extinction strain rate of the oxidizer stream $a_{e,O}$.

Unlike the results of the research done on hydrogen addition, which suggested that the influence of hydrogen to methane diffusion flames affects the extinction strain rates in a way irrespective of whether the hydrogen is added on the fuel or oxidizer side (provided that the stoichiometric mixture fraction, the adiabatic flame temperature and the ratio r of the oxidizer flux that burns hydrogen to the oxidizer flux that burns methane are constant), the methane flame under carbon monoxide addition behaves very differently.

Adding carbon monoxide to the oxidizer stream doesn't influence the oxidizer extinction strain rate whereas the CO-addition on the fuel side first increases the oxidizer extinction strain rate and then sharply reduces it after peaking out. This experimental data is qualitatively backed by computational simulations in ChemkinPro.

8 List of Figures

9 List of Tables

10 Bibliography

[1] U. Niemann, K. Seshadri and F. A. Wiliams, "Effect of Addition of a Nonequidiffusional Reactant to an Equidiffusional Diffusion Flame," *Combustion Theory and Modelling,* 9 10 2012.

[2] F. Williams, Combustion Theory, Redwood City: Addison-Wesley Publishing Company, 1985.

[3] R. Seiser, *Nonpremixed Combustion of Liquid Hydrocarbon Fuels,* Graz, 2000.

[4] A. Steynberg und M. Dry, Fischer-Tropsch Technology, Elsevier, 2004.

[5] D. Geldart, Gas Fluidization Technology, New York: John Wiley and Sons, 1986.

[6] S. Sadaka, A. Ghaly und M. Sabbah, „Two phase biomass air-steam gasification model for fluidized bed reactor (I, II, III)," *Biomass and Bioenergy 22,* pp. 439-487, 2002.

[7] S. Sadaka, Arkansas: University of Arkansas, Cooperative Extension Service Printing, FSA1051-PD-5-09N.

[8] I. K. Puri und K. Seshadri, „Extinction of diffusion flames burning diluted methane and diluted propane in diluted air," *Combustion and Flame 65,* pp. 137-150, 1986.

[9] S. Humer, *Development of a Surrogate Diesel Fuel,* Wien, Wien, 2007.

[10] J. Gore, S. Skinner, D. Stroup, D. Madrzykowski und D. Evans, „Structure and Radiation Properties of large two phase flames.," *American Society of Mechanical Engineers. Heat Transfer in Combustion Systems,* pp. 10-15, December 1989.

[11] N. Peters, *Skriptum "Technische Verbrennung",* Rheinland Westfalen: RWTH Aachen, 2012.

[12] K. Seshadri und F. Williams, „Laminar flow between parallel plates with injection of a reactant at high reynolds number," *International Journal of Heat and Mass Transfer,* pp. 251-253, 2 1978.

[13] B. J. McBride, M. J. Zehe und S. Gordon, Glenn Research Center, Cleveland, Ohio: National Aeronautics and Space Administration, 2002.

[14] I. Glassmann and R. A. Yetter, Combustion (4th Edition), San Diego, CA: Academic Press, 2008.

[15] A. S. Morris und R. Langari, Measurement and Instrumentation - Theory and Application, Elsevier, 2012.

[16] W. Payer, *Chemical-kinetic Characterization of autoignition and combustion of liquid fuels,* Vienna: Vienna University of Technology, 2002.

[17] Combustion Research Group San Diego, 16 06 2013. [Online]. Available: http://web.eng.ucsd.edu/mae/groups/combustion/mechanism.html. [Zugriff am 16 06 2013].

[18] J. Miller, „Rich methane/air flames: Burning velocities, extinction limits, and flammability limit," Sandia National Labs, Irvine, CA, 1994.

[19] Chemkin Software, „Chemkin Theory Manual," San Diego, 2012.

[20] C. R. G. San Diego, *The San Diego Mechnanism,* http://combustion.ucsd.edu/.

[21] P. Saxena, *Numerical and Experimental Studies of Ethanol Flames and Autoignition Theory for Higher Alkanes,* University of California at San Diego, Department of Mechanical and Aerospace Engineering, 2007.

[22] U.S. Department of Energy-National Energy Technology Laboratory (NETL), The Gas Turbine Handbook, National Energy Technology Laboratory, DOE, Morgantown, WV: Engineering Faculty Book Gallery, 2006.

[23] J. Warnatz, U. Maas und R. Dibble, Verbrennung. Physikalisch-Chemische Grundlagen, Modellierung und Simulation, Experimente, Schadstoffenstehung. 3. Auflage, Berlin Heidelberg New York: Springer, 2001.

[24] VDI-Gesellschaft Verfahrenstechnik und Chemieingenieurswesen, VDI-Wärmeatlas. 10. Ausgabe, Berlin Heidelberg New York: Springer, 2006.

[25] Incropera, DeWitt, Bergman und Lavine, Fundamentals of Heat and Mass Transfer. 6th Edition., Hoboken: John Wiley & Sons, 2007.

[26] B. E. Gelfand, M. V. Silnikov, S. P. Medvedev und S. V. Khomik, Thermo-Gas Dynamics of Hydrogen Combustion and Explosion, Heidelberg London New York: Springer, 2012.

[27] L. W. Eget und W. J. Alvesteffer, *ASME Fluids Engineering Division Summer Meeting,* Washington, DC: Teledyne Hastings Instrument, 1998.

[28] Teledyne Hastings Instruments, *Instruction Manual,* Hampton, Virgina: Teledyne Hastings Instruments, 2011.